

A Rich Satellite Population of the NGC 4437 Group and Implications of a Magnitude Gap for Galaxy Group Assembly History

YOO JUNG KIM,¹ JISU KANG,¹ MYUNG GYOON LEE,¹ AND IN SUNG JANG²

¹*Astronomy Program, Department of Physics and Astronomy, Seoul National University, 1 Gwanak-ro, Gwanak-gu, Seoul 08826, Republic of Korea*

²*Department of Astronomy & Astrophysics, Univ. Chicago, 5640 S. Ellis Avenue, Chicago, IL 60637, USA*

(Accepted February 24, 2022)

Submitted to ApJ

ABSTRACT

Both observations and cosmological simulations have recently shown that there is a large scatter in the number of satellites of Milky Way (MW)-like galaxies. In this study, we investigate the relation between the satellite number and galaxy group assembly history, using the r -band magnitude gap (Δm_{12}) between the first and the second brightest galaxy as an indicator. From 20 deg² of Hyper Suprime-Cam Subaru Strategic Program Wide layer, we identify 17 dwarf satellite candidates around NGC 4437, a spiral galaxy with about one-fourth of the MW stellar mass. We estimate their distances using the surface brightness fluctuation (SBF) method. Then we confirm five candidates as members of the NGC 4437 group, resulting in a total of seven group members. Combining the NGC 4437 group (with $\Delta m_{12} = 2.5$ mag) with other groups in the literature, we find a stratification of the satellite number by Δm_{12} for a given host stellar mass. The satellite number for given host stellar mass decreases as Δm_{12} increases. The same trend is found in simulated galaxy groups in IllustrisTNG50 simulations. We also find that the host galaxies in groups with a smaller Δm_{12} (like NGC 4437) have assembled their halo mass more recently than those in larger gap groups, and that their stellar-to-halo mass ratios (SHMRs) increase as Δm_{12} increases. These results show that the large scatter in the satellite number is consistent with a large range of Δm_{12} , indicating diverse group assembly histories.

Unified Astronomy Thesaurus concepts: Galaxy Groups (597); Dwarf galaxies (416); Galaxy dark matter halos (1880); Distance indicators (394); Galaxy distances (590); Luminosity Function (942)

1. INTRODUCTION

In the Λ CDM paradigm, galaxies form in the center of dark matter halos and evolve through hierarchical merging and accretion. Smaller halos that are accreted into larger halos and become gravitationally bound are called subhalos, which observationally correspond to the satellite galaxies. It is inferred that the more massive the dark matter halos are, the more abundant the satellite systems are.

This structure formation model has been tested by comparing observations with simulations. The well-known “Missing Satellites” problem (Klypin et al. 1999; Moore et al. 1999) is an example. With dark matter-only

cosmological simulations, Milky Way (MW)-like halos in the Λ CDM scenario are predicted to have far more satellites than observed around the MW and it is considered as one of the “small-scale” challenges to Λ CDM (see Bullock & Boylan-Kolchin 2017, and references therein). This motivated numerous studies of individual satellite systems, to find out whether the MW satellite population is representative among them, from the Local Volume (LV; $D < 11$ Mpc) host galaxies (e.g. M31 (see Martin et al. 2016; McConnachie 2012; McConnachie et al. 2018, for compiled data), M81 (Chiboucas et al. 2009, 2013), NGC 5128 (Centaurus A) (Crnojević et al. 2014, 2019; Müller et al. 2017, 2019), M94 (Smercina et al. 2018), M101 (Danieli et al. 2017; Bennet et al. 2017, 2019; Carlsten et al. 2019a), NGC 4258 (M106) (Spencer et al. 2014; Kim et al. 2011), NGC 628 (Davis et al. 2021)) to those in farther distances (NGC 3175 (Konda-

pally et al. 2018), NGC 2950 and NGC 3245 (Tanaka et al. 2018)).

In more recent years, statistical studies of satellites around MW-like galaxies have been carried out (Carlsten et al. 2020a,b, 2021; Wang et al. 2021; Geha et al. 2017; Habas et al. 2020; Mao et al. 2021; Roberts et al. 2021). Among them Carlsten et al. (2021) presented a study of a large sample of dwarf satellite systems around 12 LV host galaxies within the projected distance to their host galaxy (R_h) of 150 kpc, to which surface brightness fluctuation (SBF) or the tip of the red giant branch (TRGB) distances are measured. They found that the MW satellite luminosity function is typical among other MW-like LV hosts.

At farther distances beyond the LV, while it is more difficult to identify and confirm membership of faint galaxies, clear advantages exist: there are a larger number of MW-like galaxies and a smaller field of view is sufficient to survey the entire virial volume. Among others, the SAGA survey (Geha et al. 2017; Mao et al. 2021) presented a study of spectroscopically confirmed satellites with a homogeneous spatial and photometric completeness. The SAGA Stage II (Mao et al. 2021) presented 127 satellites within $R_h = 300$ kpc around 36 MW-like hosts at distance $25 \text{ Mpc} < D < 40.75 \text{ Mpc}$. They suggested that the number of satellites ($M_r < -12.3$ mag) of the MW-like hosts is remarkably varied, from zero to nine. In their sample, the MW has a typical number of satellites.

Meanwhile, several theoretical studies found that baryonic cosmological simulations produce fewer observable satellites around MW-like hosts compared with previous simulation studies, which is consistent with observations (Wetzel et al. 2016; Garrison-Kimmel et al. 2019; Fattahi et al. 2016; Sawala et al. 2016; Font et al. 2021). Also, the diversity of satellite number was shown by Engler et al. (2021) who studied satellite systems of 198 MW-like hosts found in IllustrisTNG50 (Nelson et al. 2019).

Thus, there is growing consensus between observations and simulations that the number of satellites of the MW is typical among other observed and simulated systems. Besides, a large *scatter* in the number of satellites is recognized from both approaches.

One of the causes of the large scatter might be *diverse galaxy assembly histories*. In the hierarchical structure formation scenario, it is expected that an early-formed system would have already cannibalized its massive satellite galaxies, if existed. Therefore, the early-formed system would likely have a small number of satellite galaxies with the central galaxy dominating the brightness of the group. Indeed, Mao et al. (2021) noted

that MW-mass galaxy groups with massive satellites in the SAGA survey have a larger number of satellites. In addition, Smercina et al. (2021) found a tight relationship between the mass of a galaxy’s most dominant merger and its number of satellites, using stellar halo and satellite properties of eight nearby MW-like galaxies. As a metric for the galaxy’s most dominant merger, they used either the total accreted stellar mass or the mass of the most massive satellite.

In this view, a magnitude difference, or a *magnitude gap* (Δm_{12}) between the brightest and the second brightest galaxy gives useful information about galaxy assembly history. A galaxy group with a large magnitude gap is likely to have assembled its mass at an early epoch. Indeed, fossil groups, which are massive groups observationally selected on the basis of r -band magnitude gap, $\Delta m_{12} > 2$ mag and X-ray luminosity $L_X > 10^{42} h_{50}^{-2} \text{ ergs}^{-1}$ (Jones et al. 2003), are considered to have assembled their mass earlier than non-fossil groups (D’Onghia et al. 2005) or have lacked recent infall of new massive satellites (Kundert et al. 2017) (See Aguerri & Zarattini (2021) for a recent review on fossil groups). Note that Δm_{12} is largely varied among nearby galaxy groups. While the M81 group has a massive satellite M82 and thus has a small gap, $\Delta m_{12} = 1.4$ mag (calculated from de Vaucouleurs et al. 1991), the M94 group has only faint satellites in its virial volume and thus has a very large gap, $\Delta m_{12} = 9.9$ mag (Smercina et al. 2018).

However, only a few studies have examined the observational evidence of the anticorrelation between the magnitude gap and the number of satellites (Hearin et al. 2013; Wang et al. 2021). Hearin et al. (2013) found that SDSS groups with small magnitude gaps ($\Delta m_{12} < 0.2$ mag) have a richer satellite system than large-gap groups ($\Delta m_{12} > 1.5$ mag) at fixed velocity dispersion among group members as a mass proxy, at about MW-mass range. They used a volume-limited galaxy group catalog complete down to absolute r -band magnitude $M_r = -19$ mag identified in Data Release 7 of the SDSS. Therefore, their sample does not contain large-gap groups with the second brightest galaxy fainter than $M_r = -19$ mag. This criteria would exclude most of the nearby galaxy groups with low mass. In addition, Wang et al. (2021) suggested that MW-mass galaxy groups with magnitude gaps smaller than one mag have richer satellite systems than those with larger magnitude gaps. However, most nearby galaxies have magnitude gaps larger than one mag. Therefore, to understand any relation between the magnitude gap and a large scatter in satellite number among nearby MW-like galaxies, more observations of nearby satellite

systems with various magnitude gaps as well as comparisons with simulations are required.

Here we study satellite populations of the NGC 4437 group, which has a relatively small magnitude gap ($\Delta m_{12} = 2.5$ mag) among nearby galaxy groups but larger than the previously studied regime. Then we compare the NGC 4437 group with those of other nearby galaxy groups as well as with mock galaxy groups from cosmological simulations.

NGC 4437 (=NGC 4517) is a LV spiral galaxy ($M_r = -20.71$ mag, $D = 9.28 \pm 0.39$ Mpc) with about one fourth the stellar mass of the MW, forming a pair with NGC 4592 which is a Large Magellanic Cloud (LMC)-mass dwarf spiral galaxy ($M_r = -18.23$ mag, $D = 9.07 \pm 0.27$ Mpc) (Kim et al. 2020). See Table 1 for the basic information of the two spiral galaxies. Although various surveys have detected several faint galaxies around NGC 4437 and NGC 4592, their relationship with these spiral galaxies was not defined except CGCG 014-054, a late-type dwarf galaxy at a Tully-Fisher distance $D = 9.59 \pm 1.77$ Mpc that was grouped together with the two galaxies by Karachentsev & Nasonova (2013).

In this study, we surveyed a wide area around NGC 4437 in the WIDE layer of Hyper Suprime-Cam Subaru Strategic Program (HSC-SSP, Aihara et al. 2018) and found 17 dwarf satellite candidates. To distinguish them from background galaxies in the Virgo cluster (~ 16.5 Mpc (Mei et al. 2007)), we checked their membership by measuring their SBF distances. In doing so, we present a spatially complete list of confirmed satellite galaxies around NGC 4437, complete down to $M_r \sim -11$ mag.

This paper is structured as follows. In Section 2, we describe the HSC data and our detection of dwarf satellite candidates. In §3, we present SBF distances to the dwarf satellite candidates and discuss their membership in the NGC 4437 group. In §4, we describe the spatial distribution of the NGC 4437 group in comparison with simulated galaxy groups in the IllustrisTNG50 cosmological simulation. In §5, we discuss environmental properties and the correlations between the magnitude gap, number of member galaxies, and assembly history of low-mass galaxy groups. In the final section, we summarize our main results.

2. DATA AND DWARF SATELLITE GALAXY SURVEY

We use the g - and i -band imaging data from the second public data release (Aihara et al. 2019) for the Wide layer of the HSC-SSP (Aihara et al. 2018), to search for dwarf satellite candidates around NGC 4437. The HSC

is a wide-field optical imager mounted on the 8.2m Subaru telescope. The survey consists of three layers, Wide, Deep, and UltraDeep with a 5σ photometric depth of $r \sim 26$, $r \sim 27$, and $r \sim 28$ mag, respectively.

The images from the HSC-SSP are fully reduced, sky subtracted, and coadded with the pipeline `hscPipe` designed for the LSST (Bosch et al. 2018; Ivezić et al. 2019). In `hscpipe v6`, astrometric and photometric calibrations were performed against the Pan-STARRS1 DR1 catalog (Aihara et al. 2019). Sky subtraction was carried out by two steps and Aihara et al. (2019) showed that the technique preserves low surface brightness features better than previous versions of `hscpipe`. The pixel scale of HSC images is $0.168''$ per pixel. The average seeing is $0.58''$ in i -band and $0.77''$ in g -band.

NGC 4437 is located in the WIDE12H field, one of the Wide layers of the survey. We first visually inspected the $5^\circ \times 4'$ (~ 0.8 Mpc \times 0.6 Mpc at the distance of NGC 4437) area centered on NGC 4437 to search for extended objects. We restricted our search to galaxies larger than $10''$ (450 pc at the distance of NGC 4437) by visual diameter extent because applying the SBF techniques to smaller low surface brightness galaxies would result in an insufficient S/N. Also, we ruled out galaxies that show visually too small SBFs to be at a distance of about 9 Mpc.

Due to the proximity to the Virgo cluster in the sky ($\sim 12.3^\circ$), some Virgo members may be included in this area. Among the objects of which a radial velocity can be found in NASA Extragalactic Database (NED), we excluded galaxies that have a relative radial velocity with respect to NGC 4437 $|\Delta v_{helio}| > 400$ km s $^{-1}$. As a result, we selected Dw1, Dw3, Dw4, Dw6, Dw7, Dw12, Dw13, Dw14, Dw15, and Dw16 as our initial sample. The selected satellite candidates with velocity measurements are Dw1, Dw3, Dw4, Dw6, and Dw13 (Figure 1 and Table 2). If an object does not have a velocity measurement, we consider it as a satellite candidate.

Then we performed a semi-automated detection following Carlsten et al. (2020a) to detect low surface brightness galaxies and estimate the completeness of our search. In this process, we added Dw2, Dw5, Dw8, Dw9, Dw10, Dw11, and Dw17 to the sample.

As a result, we find 17 candidate galaxies that vary in size, surface brightness, and morphology. Their locations are shown in Figure 2. Table 2 lists basic information of our candidate galaxies. The coordinates and heliocentric velocities are obtained from NASA Extragalactic Database (NED). We derived photometric properties of these galaxies from AUTO magnitudes obtained using Source Extractor (Bertin & Arnouts 1996) to the HSC images. The faintest object in r -band is

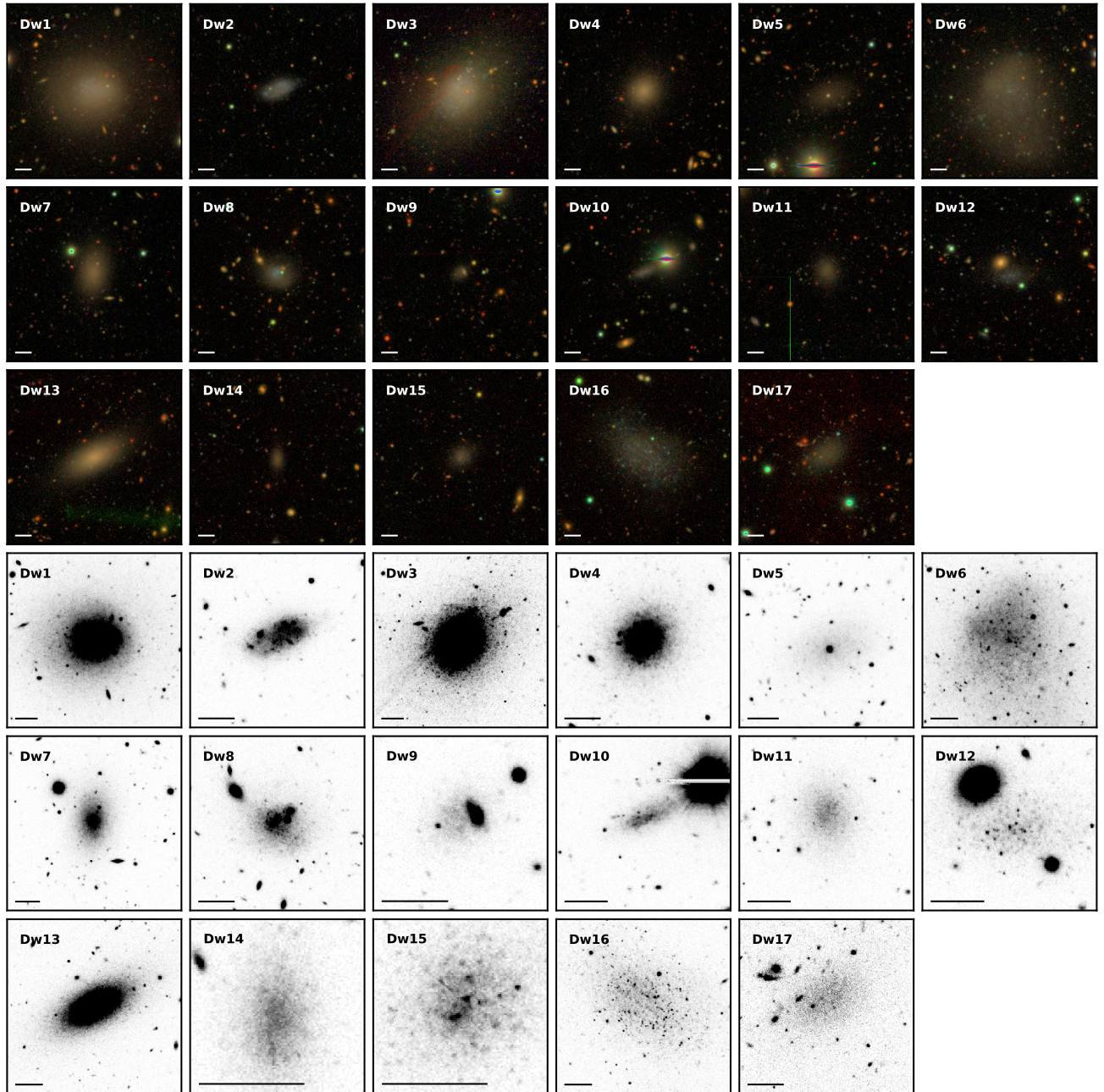


Figure 1. (Top) HSC g, r, i color images of the dwarf satellite candidate galaxies around NGC 4437. The white bars represent $10''$ length. North is up, and east to the left. (Bottom) HSC i -band zoom-in images of the sample galaxies. The black bars also represent $10''$ length.

Dw8, with $m_r = 19.58 \pm 0.02$ mag (which would correspond to $M_r \sim -10.3$ mag assuming the distance of the NGC 4437). The color range of our candidate galaxies is $0.2 \lesssim (g - i)_0 \lesssim 0.9$.

To check if our survey is complete, we injected 20,000 artificial galaxies of various structural parameters ($-10.5 \lesssim M_r \lesssim -12$ mag and $23 \lesssim \overline{\mu_{r,e}} \lesssim 26$ mag arcsec $^{-2}$) randomly into the survey field and performed semi-automated detection to find the recovery

rate. We assume that our automated detection and visual search are complete for galaxies brighter than this range. Figure 3 shows a completeness map in r -band absolute magnitude and average surface brightness within the effective radius of our sample galaxies. For comparison, dwarf galaxies in the Local Group from [McConnachie \(2012\)](#) are displayed as gray circles. Locations of our sample galaxies are overlapped with those of the Local Group dwarf galaxies. The recovery rates

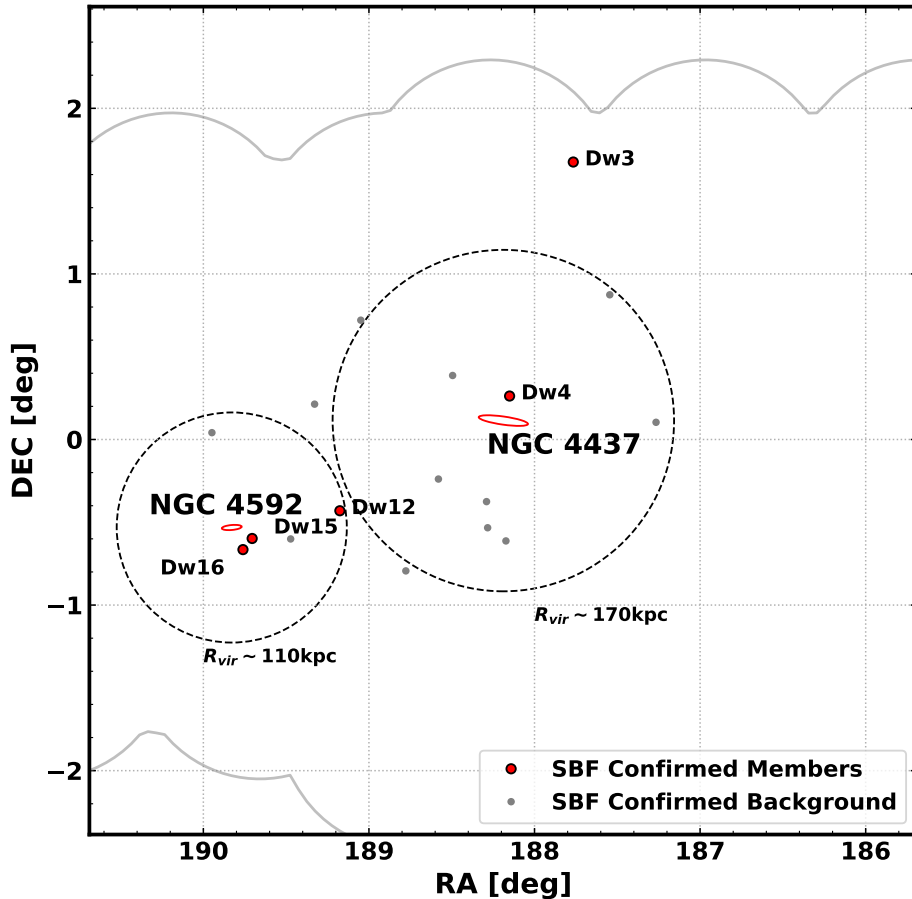


Figure 2. Location of dwarf satellite candidate galaxies of the NGC4437 group. The two spiral galaxies are shown as red ellipses. The projected virial radii (R_{vir}) of the two spiral galaxies are marked as black dashed-line circles. Red circles denote the group members, and gray dots the background galaxies. The boundary of HSC i -band footprints is displayed as gray lines.

(completeness) are indicated as colors. In general, completeness decreases as the surface brightness decreases or the total magnitude becomes fainter. More than 70% of artificial galaxies with $\overline{\mu}_{r,e} < 25$ mag arcsec $^{-1}$ and $M_r < -11$ mag are recovered.

For the following analysis, we adopt the AB magnitude in the HSC system which is similar to SDSS and CFHT systems (see Kim & Lee 2021). We correct for foreground reddening on each galaxy based on the extinction maps by Schlegel et al. (1998) and the conversion coefficients obtained by Schlafly & Finkbeiner (2011), and use a subscript 0 for corrected values.

3. GROUP MEMBERSHIP CONFIRMATION USING SBF DISTANCES

3.1. SBF Measurement

While SBF techniques have been widely used for measuring distances to bright early-type semi-resolved galaxies (e.g., Tonry & Schneider 1988; Jerjen et al. 2000; Mei et al. 2005; Mieske et al. 2007; Cantiello et al. 2018; Blakeslee et al. 2021), recent studies have shown that SBF techniques are also useful for measuring distances to dwarf galaxies with various morphological types (Carlsten et al. 2019b, 2021; Kim & Lee 2021). Subtracting the contributions from contaminating sources is trickier in the dwarf regime, but with a statistical approach for background subtraction (Carlsten et al. 2019b) and using a g -band masking threshold (Kim & Lee 2021), one can derive reliable distances to dwarf galaxies.

In order to estimate the distances to the satellite candidate galaxies and confirm their group membership, we

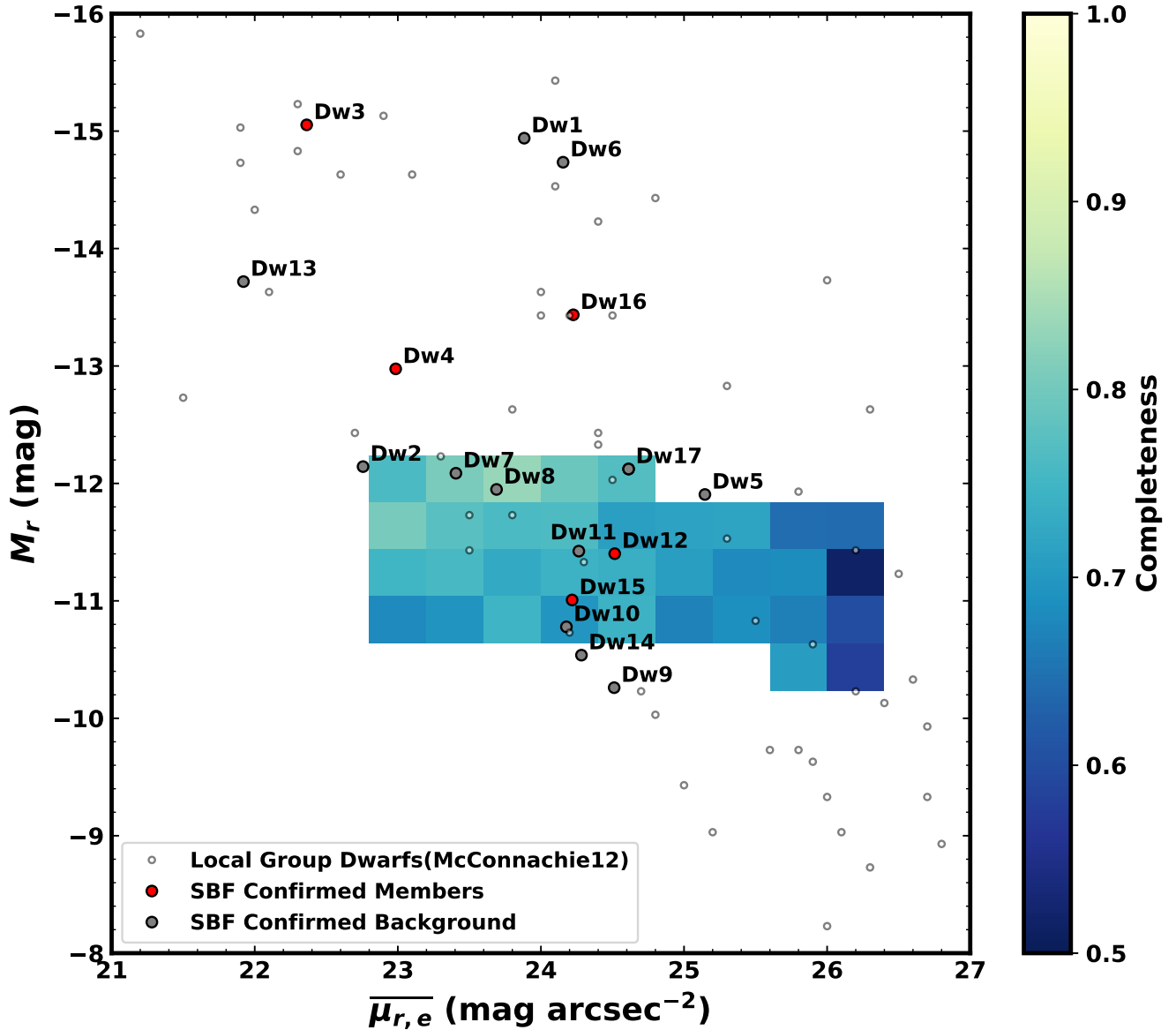


Figure 3. Completeness map in r -band absolute magnitude vs. average surface brightness within the effective radius, derived from the artificial galaxy test. The color bar represents the derived completeness. Red filled circles and gray filled circles denote confirmed group members and background galaxies, respectively. The Local Group dwarf galaxies (McConnachie 2012) are shown as gray open circles for comparison.

measure SBF magnitudes of the candidate galaxies following the methods described in Kim & Lee (2021). Here we briefly introduce the main steps of the SBF method and show examples of a dwarf spheroidal galaxy Dw4 and a blue, asymmetric irregular galaxy Dw16 in Figure 4.

In a nutshell, the SBF technique measures a PSF-scale fluctuation (dashed-line components in right panels of Figure 4) in Fourier domain of the fluctuation image, $(\text{Galaxy} - \text{Model})/\sqrt{\text{Model}}$ (Figure 4(c) and (i)), where Galaxy denotes the observed galaxy image (Figure 4(a) and (g)) and Model corresponds to the smooth

Table 1. Basic Information of NGC 4437 and NGC 4592

Name	R.A.	Decl.	V_{helio} ^a	D_{TRGB} ^b	M_{K_s} ^c	M_r ^d	M_* ^e	R_{vir} ^f	Morphology ^g
	(deg)	(deg)	(km s ⁻¹)	(Mpc)	(mag)	(mag)	(M_\odot)	(kpc)	
NGC 4437	188.189958	+0.115028	1128 ± 5	9.28 ± 0.39	-22.54	-20.71	1.27 × 10 ¹⁰	167	SA(s)cd
NGC 4592	189.828067	-0.532008	1069 ± 2	9.07 ± 0.27	-19.86	-18.23	1.07 × 10 ⁹	110	SA(s)dm

NOTE—^a From recent measurements in NED.

^b Kim et al. (2020)

^c NGC 4437: from Jarrett et al. (2003), NGC 4592: AUTO magnitude we measured from 2MASS images using SExtractor.

^d NGC 4437: converted from $M_{V_T} = -20.48$ mag (Total face-on magnitude; de Vaucouleurs et al. 1991) using $M_V = M_r + 0.23$ (Engler et al. 2021), NGC 4592: AUTO magnitude measured from HSC images using SExtractor.

^e Calculated assuming $M_*/L_{K_s} = 0.6M_\odot/L_\odot$. Note that $M_*(MW) = 5 \times 10^{10}M_\odot$ (Carlsten et al. 2021).

^f Calculated using the R_{200} versus M_{200} relation obtained from IllustrisTNG50: $\log(M_{200}) = 3 \times \log(R_{200}) + 5.03$.

^g de Vaucouleurs et al. (1991).

Table 2. A list of NGC 4437 group dwarf satellite candidates

Id	R.A.	Decl.	V_{helio}	$m_{g,0}$	$m_{r,0}$	$m_{i,0}$	$(g-i)_0$	R_e	$\overline{\mu_{i,e}}$	$t_{exp}(g/i)$	Morphology
	(deg)	(deg)	(km s ⁻¹)	(mag)	(mag)	(mag)	(mag)	($''$)	(mag $''^{-2}$)	(s)	
Dw1	187.266083	0.103806	1198 ± 13	15.15 ± 0.02	14.90 ± 0.02	14.55 ± 0.02	0.46 ± 0.02	27.9	23.5	1170/2430	Tr
Dw2	187.545510	0.873920		17.84 ± 0.02	17.69 ± 0.02	17.66 ± 0.02	0.23 ± 0.02	5.6	22.7	1170/1830	Ir
Dw3	187.765899	1.675697	1105 ± 5	15.24 ± 0.02	14.78 ± 0.02	14.60 ± 0.02	0.46 ± 0.02	14.8	22.2	1290/1060	Tr
Dw4	188.150546	0.262439	1192	17.41 ± 0.02	16.86 ± 0.02	16.60 ± 0.02	0.81 ± 0.02	7.0	22.7	1740/2070	Sph
Dw5	188.172714	-0.612622		18.58 ± 0.02	17.93 ± 0.02	17.72 ± 0.02	0.88 ± 0.02	14.0	24.9	1590/3060	Sph
Dw6	188.283101	-0.533046	750	15.58 ± 0.02	15.10 ± 0.02	14.96 ± 0.02	0.52 ± 0.02	27.8	24.0	1590/2460	Tr
Dw7	188.289818	-0.375221		18.34 ± 0.02	17.75 ± 0.02	17.49 ± 0.02	0.88 ± 0.02	6.8	23.1	1740/2260	Sph
Dw8	188.494603	0.386552		18.33 ± 0.02	17.89 ± 0.02	17.81 ± 0.02	0.54 ± 0.02	6.3	23.6	1020/1230	Tr
Dw9	188.580343	-0.238891		20.06 ± 0.02	19.58 ± 0.02	19.42 ± 0.02	0.67 ± 0.02	4.7	24.4	1170/1830	Sph
Dw10	188.777153	-0.793541		19.46 ± 0.02	19.06 ± 0.02	18.94 ± 0.02	0.54 ± 0.02	5.8	24.1	1890/2060	Ir
Dw11	189.049118	0.720478		18.88 ± 0.02	18.41 ± 0.02	18.21 ± 0.02	0.78 ± 0.02	6.8	24.1	1590/1460	Sph
Dw12	189.175590	-0.430357		18.88 ± 0.02	18.44 ± 0.02	18.28 ± 0.02	0.21 ± 0.02	8.2	24.4	1020/1230	Ir
Dw13	189.328167	0.213417	863 ± 11	16.68 ± 0.02	16.12 ± 0.02	15.84 ± 0.02	0.88 ± 0.02	8.2	21.6	1890/1060	Sph
Dw14	189.472708	-0.600737		19.84 ± 0.02	19.30 ± 0.02	19.22 ± 0.02	0.86 ± 0.02	5.2	24.2	1740/1660	Sph
Dw15	189.705284	-0.597846		19.18 ± 0.02	18.83 ± 0.02	18.67 ± 0.02	0.62 ± 0.02	5.2	24.1	2460/1490	Sph
Dw16	189.760798	-0.665024		16.82 ± 0.02	16.40 ± 0.02	16.27 ± 0.02	0.27 ± 0.02	17.0	24.1	2460/1090	Ir
Dw17	189.948333	0.041222		18.28 ± 0.02	17.71 ± 0.02	17.50 ± 0.02	0.79 ± 0.02	12.0	24.4	1170/1030	Sph

NOTE—**Galaxy References.** Dw1: 2dFGRS N320Z113 (Metcalf et al. 1989), Dw2: APMUKS(BJ) B122737.31+010900.4 (Maddox et al. 1990), Dw3: CGCG 014-054 (Zwicky et al. 1961), Dw4: MGC 34050 (Liske et al. 2003), Dw5: APMUKS(BJ) B123007.66-002012.9 (Maddox et al. 1990), Dw6: UGCA 285 (Karachentseva 1968), Dw7: APMUKS(BJ) B123035.83-000559.0 (Maddox et al. 1990), Dw10: SDSS J123506.51-004736.7 (SDSS Data Release 6), Dw11: SDSS J123611.78+004313.7 (SDSS Data Release 6), Dw12: APMUKS(BJ) B123408.34-000920.0 (Maddox et al. 1990), Dw13: MGC 35222 (Liske et al. 2003), Dw14: SDSS J123753.44-003602.6 (SDSS Data Release 6), Dw15: APMUKS(BJ) B123615.42-001923.4 (Maddox et al. 1990), Dw16: KDG 171 (Karachentseva 1968), Dw17: MGC 36065 (Liske et al. 2003)

NOTE—R.A., Decl., and V_{helio} are from NED recent values. Magnitudes are obtained from AUTO magnitude of SExtractor photometry. Magnitude errors include calibration error 0.017 mag (Aihara et al. 2019). $\overline{\mu_{i,e}}$ indicates average i -band surface brightness in half-light radius. Morphology indicates dwarf galaxy morphological types classified by our visual inspection, following Karachentsev et al. (2013) (Sph for spheroidal galaxies, Ir for irregular galaxies, and Tr for transition types between spheroidals and irregulars.)

galaxy light component (Figure 4(b) and (h)). For making smooth galaxy models, we use GALFIT (Peng et al. 2002) for the galaxies which are well described by a single Sérsic model or use median filtered images for the galaxies with an asymmetric morphology or star forming regions, with the filter size set to ten times the seeing size, following Kim & Lee (2021). Using such a filter size,

the power spectra calculated using GALFIT and median filtered image (e.g. black dots and gray crosses in Figure (e)) agree very well except for the largest scale ($k < 0.05$ pix⁻¹), which is not used for the power spectrum fitting.

We choose an optimal area for SBF calculation of a galaxy to minimize measurement errors. We measured the SBF using various annular masks (blue ellipses in

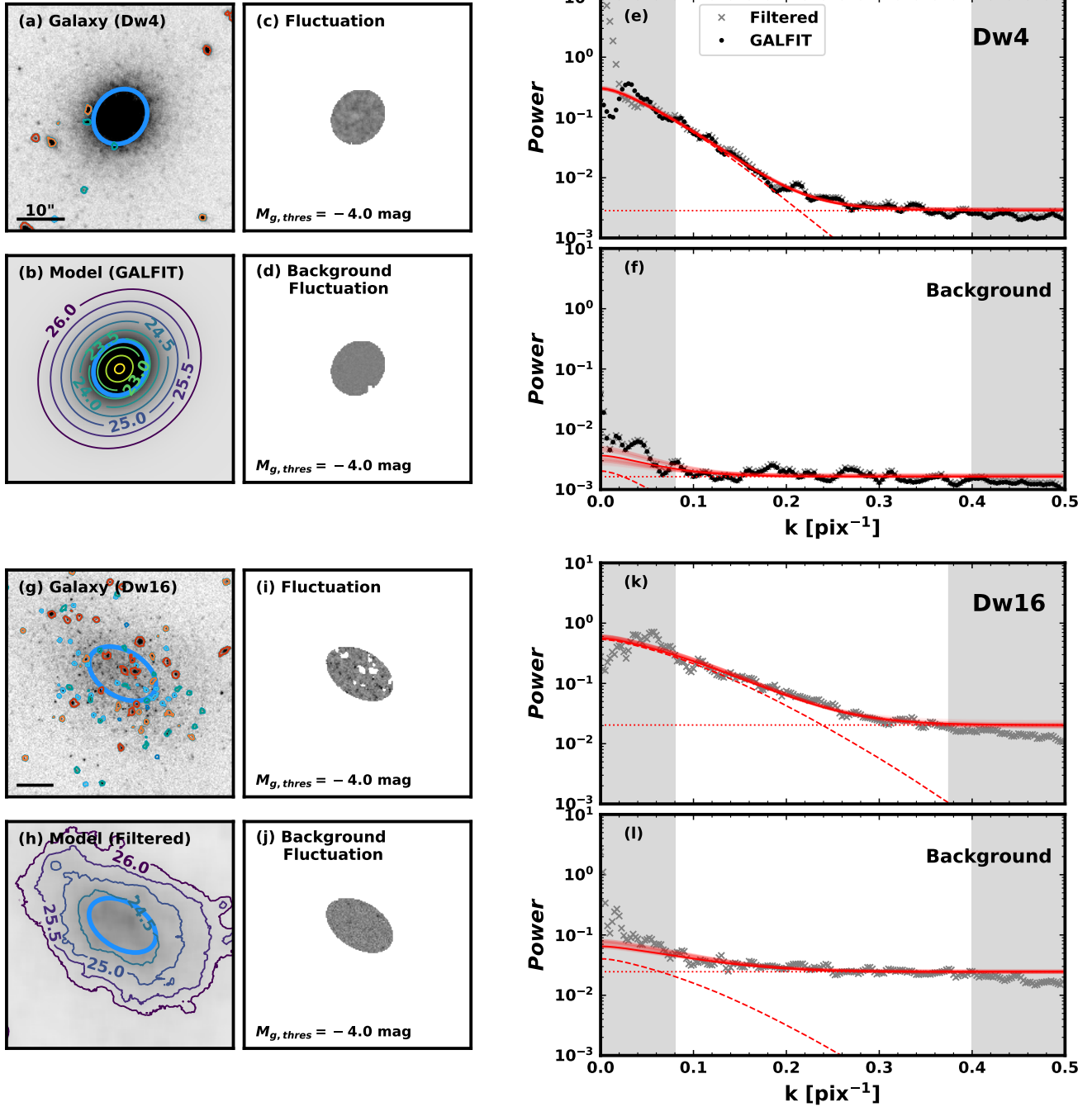


Figure 4. A summary of SBF measurement procedures for Dw4 and Dw16. The upper panels show the case of an early-type galaxy (Dw4) modelled by a single Sérsic fit, and the lower panels show the case of an asymmetric, late-type, and low surface brightness galaxy (Dw16). Panels (a) and (g) display i -band HSC images with blue ellipses representing the area used for SBF calculation. The blue, cyan, teal, orange, and red contours indicate sources masked using thresholds of $M_g = -3.5, -4.0, -4.5, -5.0,$ and -5.5 mag, respectively. Black bars represent $10''$ length. Panel (b) shows a smooth galaxy model generated using GALFIT and panel (h) shows a median filtered model image. Contours show the surface brightness as an unit of mag''^{-2} . Panels (c) and (i) are fluctuation images, which are calculated as $(\text{Galaxy} - \text{Model})/\sqrt{\text{Model}}$. Panels (d) and (j) are examples of background fluctuations sampled from a random area with no apparent bright objects and calculated as $(\text{Background})/\sqrt{\text{Model}}$. Panels (e) and (k) show azimuthally averaged power spectra of galaxy fluctuation images and fitted lines. Dashed lines and dotted lines indicate PSF-scale components and constant white noise components, respectively. Panels (f) and (l) show similar power spectra but of background fluctuations.

Figure 4(a) and (g)) and selected an area based on the galaxy's surface brightness and size. The size, color, and

mean surface brightness of the selected areas are shown in Table 3. For early-type galaxies or low surface brightness galaxies, galaxy colors and fluctuation magnitudes do not depend significantly on the choice of area. In the case of Dw3, the inner and outer regions of the galaxy show different colors, indicating different stellar populations. Therefore, we divided the galaxy into an inner region and an outer region and calculated their SBFs separately.

For subtracting fluctuations from background sources, namely foreground stars and background galaxies, we measure the fluctuations in multiple background fields as described in Carlsten et al. (2019b), and subtract the median power. Panels (d) and (j) show examples of background fluctuations and panels (f) and (l) show the corresponding power spectra. In addition, in order to mask young stellar populations which result in stochastic effects, we mask all the sources brighter than a g -band masking threshold, $M_{g,\text{thres}}$. Kim & Lee (2021) showed that the rms of the SBF calibration is the smallest in the case of $M_{g,\text{thres}} = -4.0$ mag, among the five masking thresholds $M_{g,\text{thres}} = -3.5, -4.0, -4.5, -5.0,$ and -5.5 mag.

However, without prior information of distance, it is impossible to know which apparent magnitude corresponds to $M_g = -4.0$ mag in absolute magnitude. Therefore, we try using five thresholds, $m_{g,\text{thres}} = 26.3, 25.8, 25.3, 24.8,$ and 24.3 mag, corresponding to $M_{g,\text{thres}} = -3.5, -4.0, -4.5, -5.0,$ and -5.5 mag at the distance of NGC 4437, $D = 9.28 \pm 0.39$ Mpc derived using the TRGB method (Kim et al. 2020). Note that the absolute masking thresholds change if a galaxy is located at a different distance. For example, at a distance of 11.68 Mpc (7.37 Mpc), the thresholds correspond to $-4.0, -4.5, -5.0, -5.5,$ and -6.0 mag ($-3.0, -3.5, -4.0, -4.5,$ and -5.0 mag).

Lastly, we use fluctuation – integrated color relations for dwarf galaxies in the HSC system in Kim & Lee (2021) to obtain SBF absolute magnitudes and derive distances to the satellite candidate galaxies. Kim & Lee (2021) derived fluctuation – integrated color relations for dwarf galaxies using the gi HSC data for 12 nearby dwarf galaxies of various morphological types. They presented the i -band SBF calibrations for different masking thresholds (see their Table 3): $\overline{M}_i = (-2.65 \pm 0.13) + (1.28 \pm 0.24) \times (g - i)_0$, in the case of $M_{g,\text{thres}} = -4.0$ mag which leads to the smallest rms scatter of 0.16 mag.

3.2. Group Membership Confirmation

Figure 5 shows the SBF magnitudes of the dwarf galaxies, using five different g -band masking thresh-

olds. We plot our confirmed NGC 4437 group members as orange symbols and background galaxies as blue symbols. In this subsection, we describe how we decided the membership based on SBF distances.

In each panel, we plot the SBF – integrated color relations derived by Kim & Lee (2021), assuming the distance of 9.28 Mpc (to NGC 4437), as red lines. At the 9.28 Mpc distance, the masking thresholds correspond to $M_{g,\text{thres}} = -3.5, -4.0, -4.5, -5.0,$ and -5.5 mag, respectively. With fainter $M_{g,\text{thres}}$, the slopes decrease and the y -intercepts increase. The relations assuming smaller and larger distances (7.37 Mpc, 11.68 Mpc, and 14.71 Mpc) and corresponding absolute magnitudes are also shown. If the distance to a galaxy is similar to 9.28 Mpc, its SBF magnitudes are likely to overlap with the shaded red regions. This diagram can be used for roughly estimating distances and choosing which $m_{g,\text{thres}}$ to use.

The SBF magnitudes do not differ significantly within the error range according to the choice of a masking threshold, for the galaxies in the color range $(g - i)_0 \gtrsim 0.6$ mag: for example, Dw4, Dw5, Dw7, Dw11, Dw13, Dw14, and Dw17. The latter six galaxies have significantly fainter SBFs than Dw4. They are even fainter than the relations for $D = 14.71$ Mpc. Thus, they are likely Virgo members, not members of the NGC 4437 group.

In the bluer colors, the SBF magnitudes vary with the choice of a masking threshold. Therefore, deciding the membership of galaxies with bluer colors is more difficult. For instance, it seems that SBF magnitudes of Dw1 and Dw6 are fainter than the galaxies with orange symbols for $m_{g,\text{thres}} = 26.3$ mag, but the differences decrease at brighter masking thresholds. However, in this case, deciding on a bright masking threshold is not recommended because the thresholds correspond to brighter absolute magnitudes if they are truly located behind the distance of NGC 4437 and thus young stellar populations might not have been properly masked. We decide that they are likely background objects, based on the fact that SBF magnitudes of Dw1 agree with the relations for 11.68 Mpc and those of Dw6 with 14.71 Mpc in the threshold range $m_{g,\text{thres}} \geq 25.3$ mag.

The SBF magnitudes of the Dw3 inner field and Dw12 seem to be slightly brighter than the other three galaxies with orange symbols. If they are located in front of NGC 4437, it would be better to refer to the cases for brighter masking thresholds than fainter thresholds. The SBF magnitudes of Dw12 overlap with the red shaded regions for the cases of $m_{g,\text{thres}} = 24.8$ and 24.3 mag, so we decide that it is likely a member of the NGC 4437 group. For Dw3, while the SBF magni-

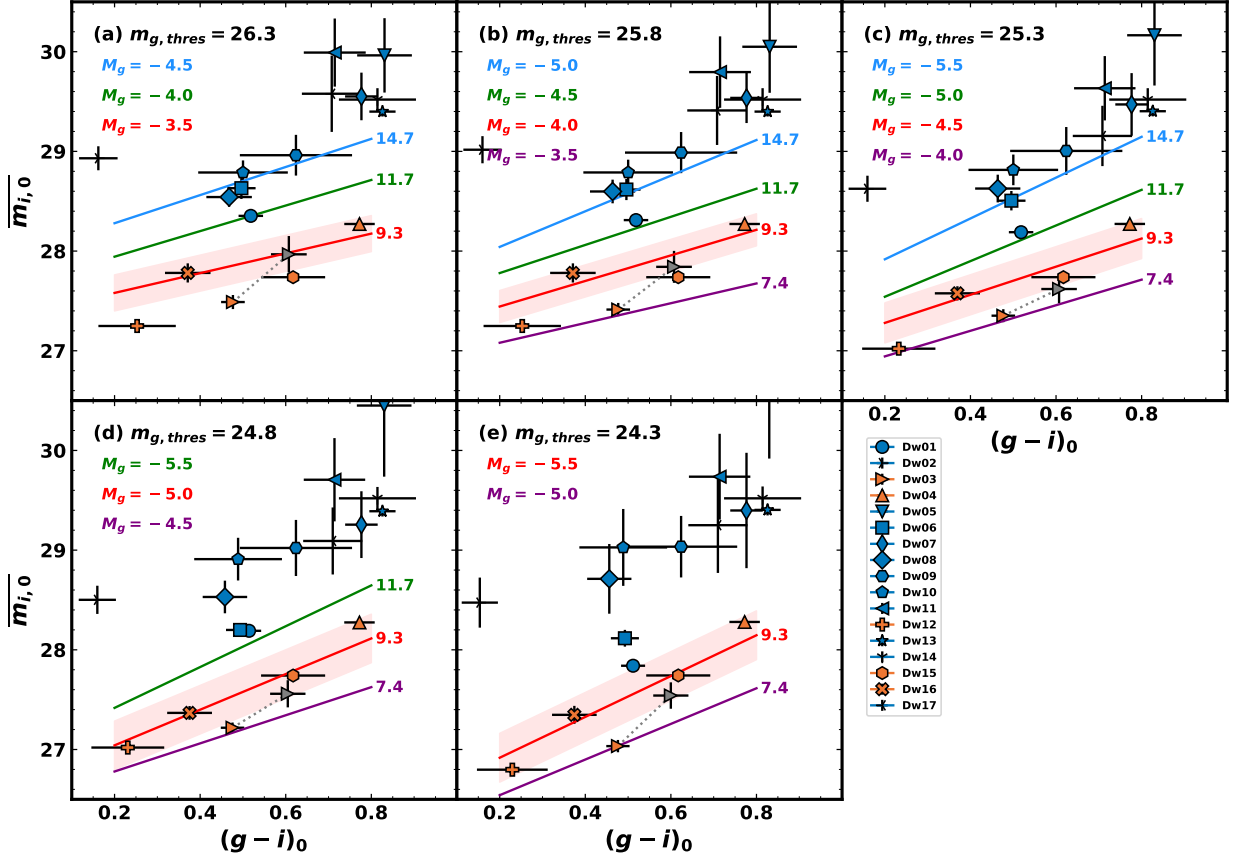


Figure 5. SBF magnitudes of the NGC 4437 group candidates, with five different g -band masking thresholds, $m_{g,\text{thres}} = 26.3, 25.8, 25.3, 24.8,$ and 24.3 mag. Assuming the 9.28 Mpc distance (to NGC 4437), the thresholds correspond to $M_{g,\text{thres}} = -3.5, -4.0, -4.5, -5.0,$ and -5.5 mag, respectively. Red lines indicate the SBF magnitude – integrated color relation in Kim & Lee (2021) assuming the 9.28 Mpc distance, for $M_{g,\text{thres}} = -3.5, -4.0, -4.5, -5.0,$ and -5.5 mag, from the left to the right. The red shaded regions represent the rms scatter of the calibrations. Five galaxies (Dw3, Dw4, Dw12, Dw15, Dw16) of which SBF magnitudes generally overlap with the shaded red regions are indicated as orange symbols, and the other 12 galaxies as blue symbols. The gray symbol indicates SBF magnitude measured from the outer region of Dw3. The SBF magnitude – integrated color relations assuming the 11.68 Mpc distance are shown as orange lines. At the distance of 11.68 Mpc, the masking thresholds correspond to $M_{g,\text{thres}} = -4.0, -4.5, -5.0, -5.5$ and -6.0 mag, respectively. Likewise, the green lines and brown lines correspond to the relations assuming the 14.71 Mpc distance and 7.37 Mpc distance, respectively.

tudes of the inner field shows better agreement with the case of $D = 7.37$ Mpc instead of $D = 9.28$ Mpc, the outer field shows better agreement with $D = 9.28$ Mpc. Thus membership confirmation based on SBF distances is more ambiguous. Fortunately, the velocity of Dw3 ($v_h = 1105 \pm 5$ km s $^{-1}$) is measured to be close to that of NGC 4437 ($v_h = 1128 \pm 5$ km s $^{-1}$) (see v_{helio} in Table 1 and 2) and we conclude that it is a likely member of the NGC 4437 group.

Figure 6 shows (a) distances, (b) SBF magnitudes, (c) distance measurement errors, and (d) total distance errors of the five likely members for five masking thresholds. $M_{g,\text{thres}}$ is calculated assuming 9.28 Mpc distance. Except for Dw3(outer region) and Dw15, distances do not vary systematically with choice of masking thresh-

olds. In the case of the outer region of Dw3, the systematic trend arises from varying apparent SBF magnitudes. On the other hand, SBF magnitudes of Dw15 are constant but the difference comes from calibrations. In the panel (c), we display the measurement errors in Mpc. Measurement errors are the sum of power spectrum fitting errors and the background subtraction errors. Large errors in Dw3(outer region) and Dw16 are due to increased stochasticity in background subtraction in low surface brightness region. In the panel (d), we show total errors, the sum of measurement error and the calibration error. Calibration errors dominate total errors. The calibration error is the smallest when using $M_{g,\text{thres}} = -4.0$, which is also reflected in total errors. We select $M_{g,\text{thres}} = -4.0$ for our final choice

Table 3. SBF Results of NGC 4437 Group Candidates

Name	Annulus	$g - i$	$\bar{\mu}_i$	Distance ($D \pm \epsilon_{stat} \pm \epsilon_{calib}$) ^a	$M_{g,thres}$ ^b	σ_D ^c	Membership
	($''$)	(mag)	(mag $''^{-2}$)	(Mpc)	(mag)	(Mpc)	
Dw1	0.0 - 10.8	0.52 ± 0.03	22.6	$12.13 \pm 0.29 \pm 1.12$	-4.5	0.25	N
Dw2	0.0 - 11.3	0.16 ± 0.04	23.6	$23.82 \pm 1.49 \pm 2.67$	-5.0	1.48	N
Dw3 _{inner}	0.0 - 15.5	0.48 ± 0.03	22.4	$7.74 \pm 0.24 \pm 0.57$	-4.0	0.09	Y
Dw3 _{outer}	15.5 - 25.2	0.61 ± 0.04	23.7	$8.75 \pm 0.65 \pm 0.65$	-4.0	0.46	
Dw4	0.0 - 6.5	0.77 ± 0.04	22.7	$9.69 \pm 0.17 \pm 0.72$	-4.0	0.05	Y
Dw5	0.0 - 11.5	0.83 ± 0.06	24.8	$22.06 \pm 4.69 \pm 2.47$	-5.0	0.68	N
Dw6	0.0 - 14.4	0.50 ± 0.03	23.8	$15.03 \pm 0.73 \pm 1.68$	-5.0	0.31	N
Dw7	0.0 - 15.8	0.78 ± 0.04	24.0	$18.21 \pm 2.12 \pm 2.04$	-5.0	0.34	N
Dw8	0.0 - 9.0	0.46 ± 0.05	24.0	$15.29 \pm 0.84 \pm 1.71$	-5.0	0.82	N
Dw9	0.0 - 5.4	0.62 ± 0.13	24.6	$16.04 \pm 1.52 \pm 1.80$	-5.0	0.42	N
Dw10	4.3 - 8.6	0.50 ± 0.10	24.7	$16.20 \pm 0.96 \pm 1.81$	-5.0	0.60	N
Dw11	0.0 - 5.4	0.71 ± 0.07	24.2	$21.59 \pm 3.56 \pm 2.42$	-5.0	1.31	N
Dw12	0.0 - 7.2	0.25 ± 0.09	24.4	$8.22 \pm 0.26 \pm 0.61$	-4.0	0.39	Y
Dw13	0.0 - 10.8	0.83 ± 0.03	22.4	$16.39 \pm 0.37 \pm 1.84$	-5.0	0.12	N
Dw14	0.0 - 5.4	0.81 ± 0.09	24.1	$17.52 \pm 0.92 \pm 1.96$	-5.0	0.12	N
Dw15	0.0 - 6.1	0.62 ± 0.07	24.2	$8.31 \pm 0.16 \pm 0.61$	-4.0	0.17	Y
Dw16	0.0 - 10.8	0.37 ± 0.05	24.2	$9.80 \pm 0.43 \pm 0.72$	-4.0	0.37	Y
Dw17	0.0 - 9.7	0.72 ± 0.07	24.2	$18.05 \pm 2.88 \pm 2.02$	-5.0	1.31	N

^a ϵ_{stat} includes measurement errors, the sum of background subtraction and fitting errors. ϵ_{calib} includes calibration errors.

^b Indicates masking threshold for the adopted calibration in Kim & Lee (2021).

^c Standard deviations of the SBF distances using multiple masking thresholds and calibrations.

of distances. For Dw3, where measured SBF distance is slightly different when using inner and outer regions, we adopt the average value 8.24 ± 0.96 Mpc.

Table 3 lists distances calibrated using $m_{g,thres} = 25.8$ mag. For the five likely members, we assume that the masking threshold corresponds to $M_{g,thres} = -4.0$ mag and apply the calibration for such threshold, $\bar{M}_i = (-2.65 \pm 0.13) + (1.28 \pm 0.24) \times (g - i)_0$ (rms = 0.16 mag). For the other likely background objects, we use calibrations for other thresholds depending on their SBF magnitudes. σ_D indicates standard deviations of SBF distances using multiple masking thresholds. Note that σ_D is generally negligible compared to calibration errors.

Figure 7 shows the distances and their error ranges of the dwarf galaxies. While 2σ distance range of the five likely members (Dw3, Dw4, Dw12, Dw15, and Dw16) includes the distance of NGC 4437, 9.28 Mpc, that of the other galaxies does not. Adopting the criterion used by Carlsten et al. (2019a) and Carlsten et al. (2021), which is confirming a dwarf as a background object whose 2σ distance lower bound is beyond the distance of the host, we consider these twelve galaxies as background galaxies. Note that all the galaxies we newly added by the automated detection are confirmed as background galax-

Table 4. Confirmed Members of the NGC 4437 Group

Name	M_r (mag) ^a	Distance (Mpc)	V_{helio} (km s $^{-1}$)
NGC 4437	-20.71	9.28 ± 0.39	1128 ± 5
NGC 4592	-18.23	9.07 ± 0.27	1069 ± 2
Dw3	-15.05	8.24 ± 0.96	1105 ± 5
Dw16	-13.44	9.80 ± 0.95	
Dw4	-12.98	9.69 ± 0.74	1192
Dw12	-11.40	8.22 ± 0.66	
Dw15	-11.01	8.31 ± 0.63	

^a For the dwarf galaxies, distances are assumed to be at the distance of NGC 4437, 9.28 Mpc.

ies, indicating that our initial visual inspection was conservative. Table 4 lists the confirmed members of the NGC 4437 Group in the order of absolute magnitudes.

Among our likely members, Dw15 has the faintest r -band magnitude ($M_r = -11.0$ mag). We assume that our search is complete at least down to $M_r = -11$ mag, among the galaxies with sufficient surface brightness to apply the SBF method.

4. SATELLITES BEYOND THE VIRIAL RADIUS

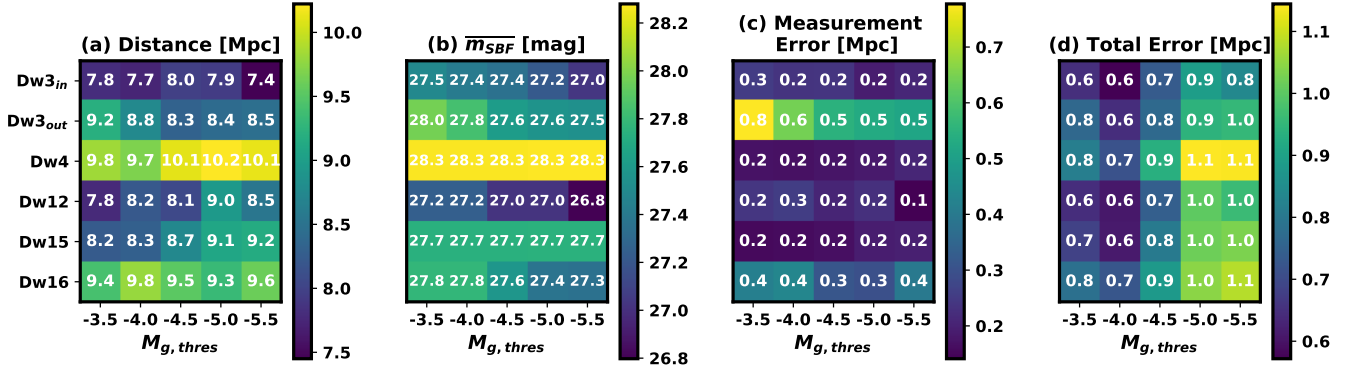


Figure 6. (a) SBF distances, (b) SBF magnitudes, (c) measurement errors of SBF distances, and (d) total SBF distance errors of the five likely members for five masking thresholds. The values of $M_{g, \text{thres}}$ are calculated assuming 9.28 Mpc distance.

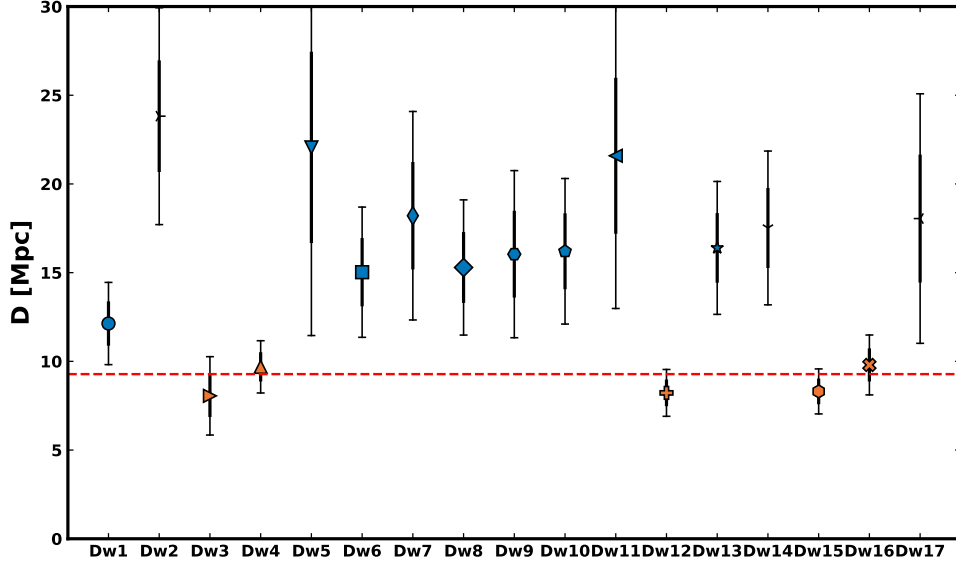


Figure 7. SBF distances of the satellite candidate galaxies (orange symbols for the group members and blue symbols for the non-group members). Bold and light error bars indicate 1σ and 2σ uncertainty ranges. The red dashed line denotes the distance of NGC 4437.

In the previous sections, we identified dwarf satellite candidates in about $5^\circ \times 4^\circ$ area around NGC 4437 and found that seven galaxies (NGC 4437, NGC 4592, Dw3, Dw4, Dw12, Dw15, and Dw16) are members of the NGC 4437 group. In this section, we describe the spatial distribution of the galaxies in the NGC 4437 group and discuss it using simulated galaxy groups in IllustrisTNG50.

4.1. Spatial Distribution of the NGC 4437 Group

In Figure 2, we plot the spatial distribution of the likely members of the NGC 4437 Group as red symbols. Black dashed circles indicate virial radii of NGC 4437 and NGC 4592, 170 kpc (1°) and 110 kpc (0.7°). These values are derived by three steps: (1) converting K_s -band magnitudes to stellar masses assuming $M_*/L_{K_s} = 0.6M_\odot/L_\odot$, (2) assuming halo masses $5.3 \times 10^{11}M_\odot$ and $1.5 \times 10^{11}M_\odot$, respectively, based on the stellar to halo mass ratio from Behroozi et al. (2013) (0.024 and 0.007, respectively), and (3) deriving

virial radii from the R_{200} versus M_{200} relation obtained from IllustrisTNG50 (see Section 5.2) group catalogs, $\log(M_{200}) = 3 \times \log(R_{200}) + 5.03$. The parameters are listed in Table 1. Thus, our field of view covers approximately $5R_{vir} \times 4R_{vir}$ area centered on NGC 4437. This spatial coverage is wider than most observational studies of nearby galaxy groups, which restrict the group members to those within the projected virial radius (e.g. Carlin et al. 2016; Smercina et al. 2018; Davis et al. 2021; Carlsten et al. 2021; Mao et al. 2021).

The distance between NGC 4437 and NGC 4592 is about two times the virial radius of NGC 4437. Dw4 is in the virial volume of NGC 4437 and Dw12, Dw15, and Dw16 are located within the virial radius of NGC 4592. Dw3 is relatively isolated, being outside of the virial radius of both NGC 4437 and NGC 4592. If we restrict the group members to those within the projected virial radius (dashed lines in Figure 2), we should regard NGC 4437 and NGC 4592 as primary galaxies of separate groups. However, given that their observed radial velocities are remarkably similar ($\Delta V_{helio} \sim 60 \text{ km s}^{-1}$), it is likely that they are gravitationally bound. However, the velocity information is not conclusive because we do not know their tangential velocities. To decide whether or not to view the two galaxies as consisting a single group, in the next subsection, we check spatial extent and velocity distributions of galaxies in the IllustrisTNG50 mock galaxy groups, especially for if the galaxies located outside the virial radius of the host galaxies are truly gravitationally bound.

4.2. IllustrisTNG50 Mock Galaxy Groups

We use group catalogs from the IllustrisTNG50 project (Marinacci et al. 2018; Naiman et al. 2018; Nelson et al. 2018; Pillepich et al. 2018; Springel et al. 2018; Nelson et al. 2019) to select mock galaxy groups. IllustrisTNG is a suite of large-scale cosmological galaxy formation simulations, with three different volumes and resolutions (TNG50, TNG100, and TNG300). We choose the smallest resolution TNG50, which has the baryonic mass resolution $m_b = 8.5 \times 10^4 M_\odot$. The group catalog includes halos determined by friends-of-friends (FoF) algorithm with a linking length $b = 0.2$ and substructures (subhalos) identified by Subfind algorithm (Springel et al. 2001; Dolag et al. 2009).

4.2.1. Subhalo Selection

We only consider subhalos with SubhaloFlag = 1 and instantaneous dark matter fraction larger than 10%, to exclude non-cosmological objects that are fragments or clumps produced through baryonic processes in already formed galaxies (Nelson et al. 2019). We also restrict our analysis to luminous subhalos with stellar masses

of at least $M_*(< 2R_{\text{eff}}) = 5 \times 10^6 M_\odot$ measured within twice the stellar half-mass radius following Engler et al. (2021), in order to avoid resolution effects. This stellar mass threshold roughly corresponds to $M_r \sim -11$ mag, similar to the completeness limit of our search of NGC 4437 group satellites. In IllustrisTNG50, 21864 subhalos satisfy both criteria. Black lines in Figure 8a shows a stellar mass function of the selected subhalos.

4.2.2. Galaxy Group Selection

Next, we select galaxy groups based on two criteria. First, we limit our analysis to FoF groups with a total stellar mass larger than $10^9 M_\odot$. In IllustrisTNG50, 1928 FoF groups satisfy this mass limit. Red dotted lines in Figure 8 shows the host galaxy stellar mass function of such groups. Here we define a host galaxy as the most massive subhalo among subhalos in a FoF group and satellite galaxies as the other subhalos. Second, we only consider galaxy groups that have at least one satellite galaxy brighter than $M_r = -11$ mag. That is, the galaxy groups with at least one subhalo (other than the host subhalo itself) that satisfies the subhalo selection criteria. Red solid lines in Figure 8 display the host galaxy stellar mass function of the 661 groups that satisfy both the two criteria. Then we classify selected FoF groups according to host stellar mass: low-mass NGC 4437 group-like groups ($9.9 < \log[M_*/M_\odot] < 10.3$; $N = 203$), MW-like groups ($10.3 < \log[M_*/M_\odot] < 10.9$; $N = 237$), and massive groups ($10.9 < \log[M_*/M_\odot] < 11.5$; $N = 96$). These are indicated as vertical colored bars in the right panel (Figure 8b).

4.2.3. Spatial Extent of Simulated Galaxy Groups

Now we define two quantities to describe the spatial extent of simulated galaxy groups: D_{max} and D_{12} . D_{max} of a galaxy group is the distance between the host galaxy and the farthest satellite galaxy ($M_r < -11$ mag). D_{12} of a galaxy group is the distance between the host galaxy and the second brightest member galaxy. For the NGC 4437 group, $D_{12} = 0.29_{-0.03}^{+0.30}$ Mpc $\sim 1.7_{-0.2}^{+1.8} R_{200}$ (Kim et al. 2020). D_{max} is highly uncertain because of the wide distance error ranges in dwarf galaxies.

In Figure 9 we plot the histogram of two quantities in units of the virial radius R_{200} . The solid lines indicate all the selected galaxy groups and the filled lines display NGC 4437 group-like galaxy groups, the galaxy groups of which host galaxies have similar stellar masses with NGC 4437 ($9.9 < \log[M_*/M_\odot] < 10.3$). About half of the NGC 4437 group-like galaxy groups have D_{max} larger than R_{200} and about 10% of them outside $2R_{200}$. About 30% of the NGC 4437 group-like galaxy groups have the second brightest member galaxy outside R_{200}

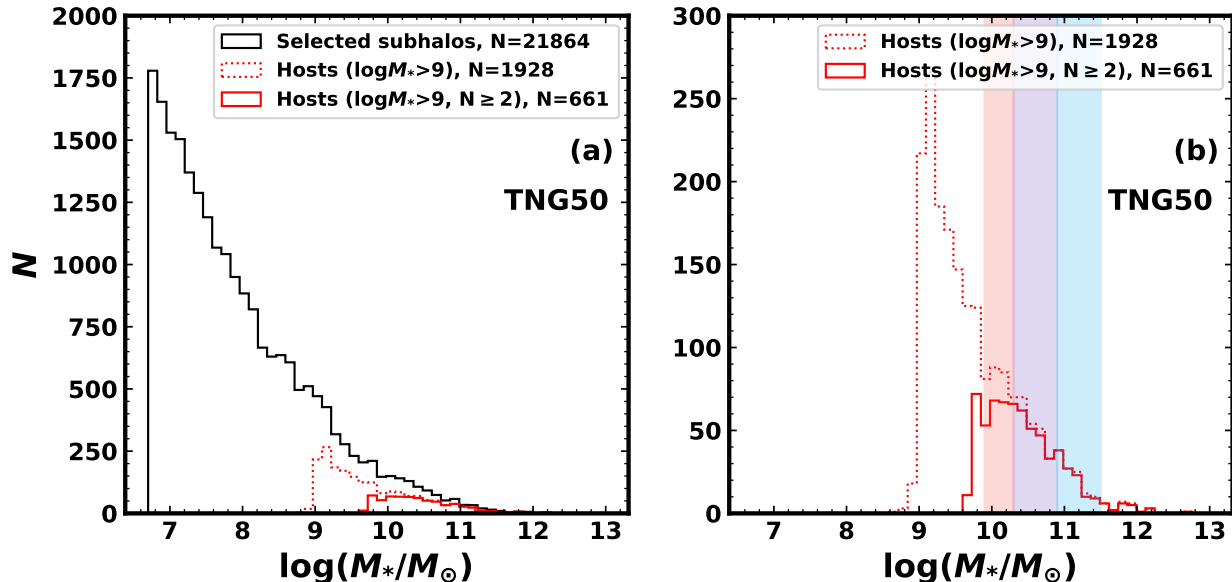


Figure 8. (Left) Stellar mass function of IllustrisTNG50 host subhalos (galaxies) in mock galaxy groups. Black lines display host subhalos with at least $5 \times 10^6 M_\odot$ within twice the stellar half-mass ratio. Red dotted lines indicate galaxy groups larger than $10^9 M_\odot$ and red solid lines show those with at least one more subhalo other than the host subhalo brighter than $M_r = -11$ mag among them. (Right) A zoomed-in version of the left figure. Red, purple, and blue vertical ranges indicate classification of galaxy groups according to host stellar mass: NGC 4437 group-like, MW-like, and massive groups.

and 10% outside $2R_{200}$. This shows that although a majority of groups have D_{max} and D_{12} within R_{200} , a significant fraction of satellite galaxies lie outside the R_{200} , like the case for NGC 4437 and NGC 4592.

To test if these large-distance satellite galaxies are truly bound to the host galaxies, we check their relative velocities. We find that a majority (75%) of the second brightest member galaxies of galaxy groups with $D_{12} > R_{200}$ are infalling toward their host galaxies. The other 25% of them are receding from the host galaxy but have a velocity smaller than the escape velocity. Thus, it is likely that second brightest member galaxies outside the R_{200} will get closer to the primary galaxy and shortly become close satellites. Therefore we conclude that galaxies grouped as a FoF halo in the IllustrisTNG50 are bound, even though their separations are large.

To summarize, we find that a significant fraction of subhalos in a FoF group in the IllustrisTNG50 simulation are located outside the R_{200} and that they are still bound to the host galaxy. Thus, we decide to view the NGC 4437 group, which has $D_{12} = 1.7R_{200}$, as a single group.

5. DISCUSSION

In this section, we discuss the properties of the satellites of the NGC 4437 group, in comparison with previ-

ous studies on low-mass and MW-mass galaxy groups and with cosmological hydrodynamic simulations.

5.1. Environmental Quenching of Satellites

Star formation properties of our satellite galaxies imply that environmental quenching has affected them. The two satellite galaxies (Dw4 and Dw15) that are located in the shortest projected distance to NGC 4437 and NGC 4592, are dwarf spheroidal galaxies with red colors ($(g-i)_0 = 0.81 \pm 0.02$ and 0.62 ± 0.02 mag, respectively), implying that they consist of old stellar populations. On the other hand, the satellites located farther from the pair of spiral galaxies (Dw3, Dw12, and Dw16) are late-types with bluer colors ($(g-i)_0 < 0.5$ mag) and ultraviolet flux is detected from GALEX images of them. This is consistent with earlier finding that the morphological type of satellite galaxies around the MW, M31, M81 and M101 shows a strong correlation with projected distances from their host galaxies (Einasto et al. 1974), and with color-projected distance relation well-known for galaxy clusters (Dressler 1980) and the Local Group (van den Bergh 1994). Recent studies show that similar trends exist even for low-mass galaxy groups (Carlin et al. 2021; Davis et al. 2021). The satellite system of the NGC 4437 group supports the idea that environmental quenching plays a role even for low-mass galaxy groups where lower ram pressure and tidal fields are expected.

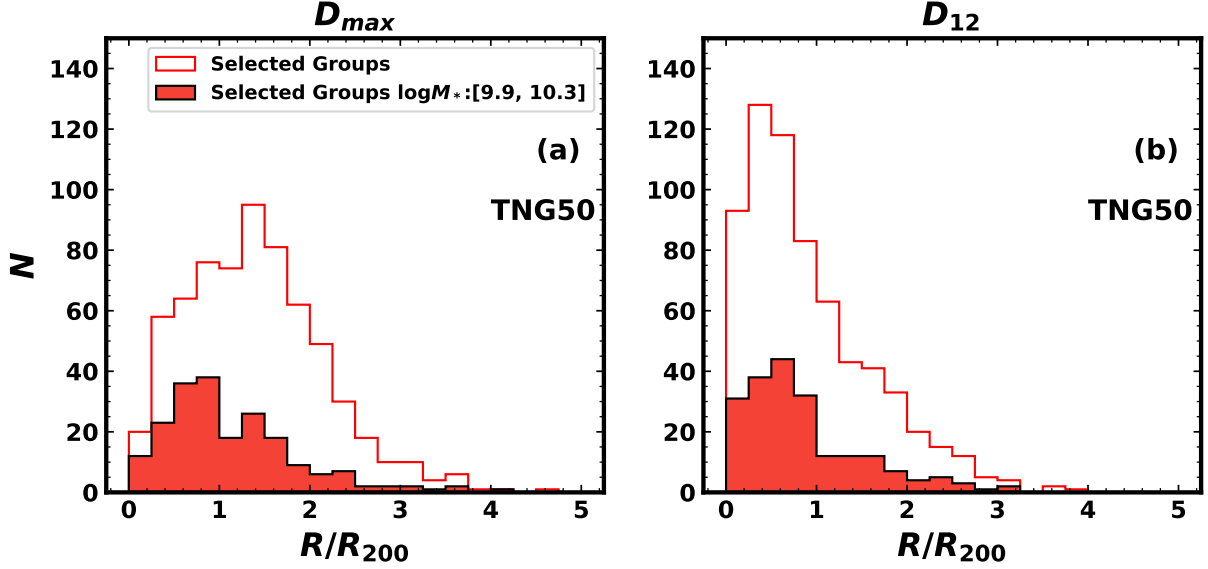


Figure 9. (Left) D_{max} and (Right) D_{12} distribution of the selected mock galaxy groups in IllustrisTNG50. Red solid lines show all the selected galaxy groups and red filled bars with black edges display NGC 4437 group-like galaxy groups. Note that a significant fraction of satellite galaxies is located outside the virial radius.

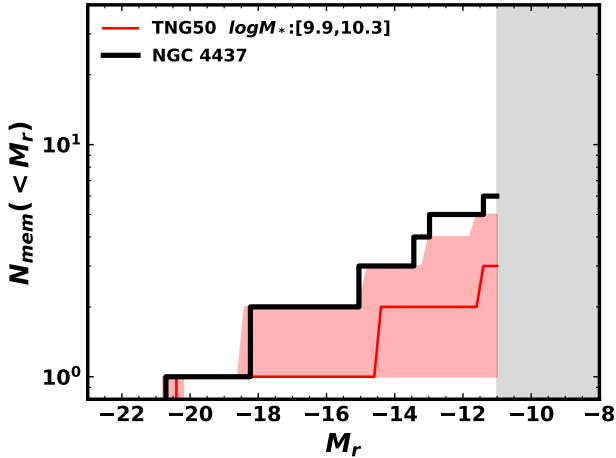


Figure 10. Member galaxy LFs of the NGC 4437 group (thick black solid line) in comparison with simulated low-mass groups with $\log[M_*/M_\odot] = 9.9 - 10.3$ in IllustrisTNG50.

5.2. Satellite Luminosity Functions, Number of Member Galaxies, and the Magnitude Gap

There are seven galaxies ($M_r < -11$ mag) confirmed as members of the NGC 4437 group. In this subsection, we compare the spatially complete satellite population of the NGC 4437 group with the mock galaxy groups in the IllustrisTNG50 cosmological simulation and with other observed galaxy groups.

Figure 10 displays the observed cumulative luminosity function (LF) of the members in the NGC 4437 group

(thick black solid line) in comparison with the median LF of simulated NGC 4437 group-like galaxy groups (defined in Section 4.2). The median and $\pm 1\sigma$ range of the LF of simulated galaxy groups are shown as a red line with a red shaded region. The photometric limit of this study, $M_r \sim -11$ mag, is indicated by the gray shaded region. The NGC 4437 group has a relatively large satellite population compared to the simulated galaxy groups with a similar host stellar mass.

In addition, the median of the M_r of the second brightest galaxy in the simulated galaxy groups is about $M_r \sim -14.5$ mag. NGC 4592, the second brightest galaxy in the NGC 4437 group, is relatively bright (-18.2 mag) among the NGC 4437 group-like simulated galaxy groups. This means that it has a relatively small *magnitude gap* ($\Delta m_{12} = 2.5$ mag) between the host galaxy (NGC 4437) and the brightest satellite galaxy (NGC 4592) compared to the simulated galaxy groups.

Previously studied observational evidence of the anticorrelation between the Δm_{12} and the number of satellites is based on the comparison between galaxy groups with a very small Δm_{12} ($\Delta m_{12} < 0.2$ mag for Hearin et al. (2013) and $\Delta m_{12} < 1$ mag for Wang et al. (2021)) and the rest. To check whether the anticorrelation extends to a larger gap regime for low-mass galaxy groups, we classify the simulated galaxy groups into five groups by Δm_{12} , $0 < \Delta m_{12} < 1$, $1 < \Delta m_{12} < 3$, $3 < \Delta m_{12} < 5$, $5 < \Delta m_{12} < 7$, and $7 < \Delta m_{12} < 9$.

Figure 11 displays the number of member galaxies of the group, N_{mem} as a function of (a) host galaxy stel-

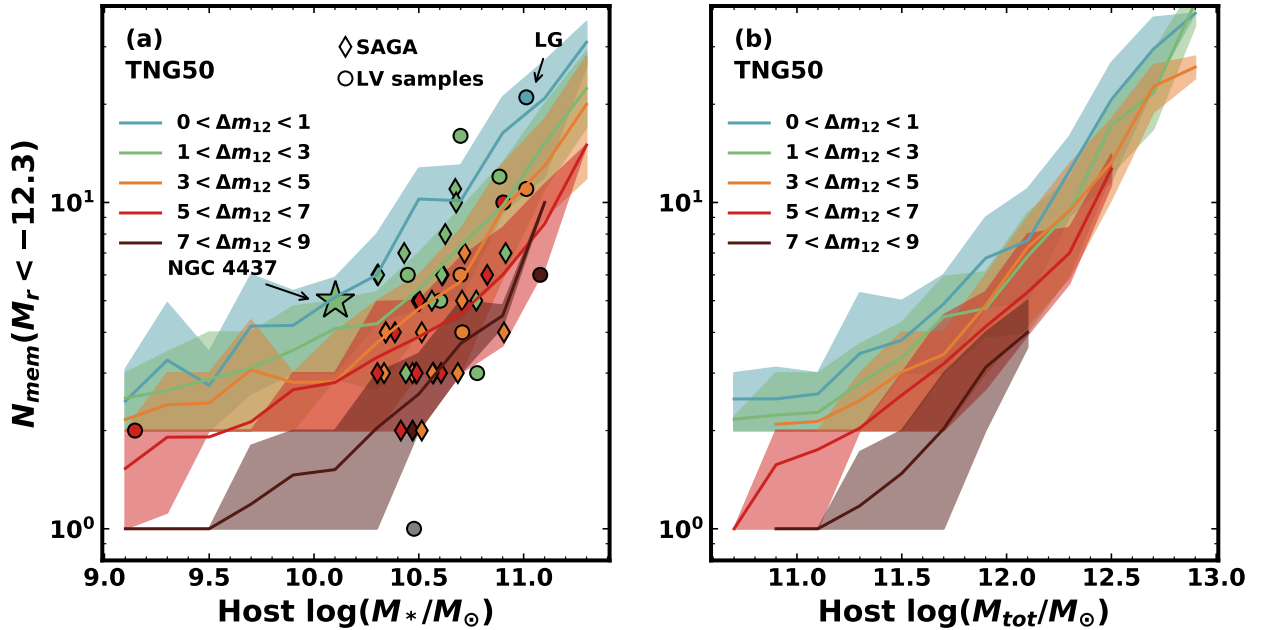


Figure 11. (a) Relations between the number of member galaxies (N_{mem}) brighter than $M_r = -12.3$ mag and stellar mass of the host galaxies from the IllustrisTNG50 simulation. Simulated galaxy groups are classified into five groups by their Δm_{12} and their average and 1σ range of the N_{mem} are displayed as lines with shaded regions. The star symbol indicates the NGC 4437 group. Diamond symbols and circle symbols show the data from the SAGA survey (Mao et al. 2021) and the LV sample (Carlsten et al. 2021; Carlin et al. 2021; McConnachie 2012; McConnachie et al. 2018). Note the stratification of the N_{mem} by Δm_{12} for a given host stellar mass. (b) Relations between N_{mem} ($M_r < -12.3$ mag) and total mass of the host galaxies derived from the IllustrisTNG50 simulation.

lar mass and (b) host galaxy total mass from the IllustrisTNG50 simulation. Here we consider the satellites brighter than $M_r = -12.3$ mag in order to match the magnitude limit of the SAGA survey (Mao et al. 2021) which will be described below. The five groups classified by Δm_{12} are shown by different colors (the bluer color for the smaller Δm_{12}). Two correlations are seen in these figures. First, the positive correlation between N_{mem} and host galaxy stellar mass is seen in the simulated groups. The correlation is tighter against the total mass (including the dark matter halo mass) of the host galaxy. In addition, the number of satellites from the simulated groups shows a clear stratification in both Figure 11(a) and (b): galaxy groups with a smaller Δm_{12} have a larger N_{mem} . Note that the stratification of the same Δm_{12} exists across a broad Δm_{12} range.

We overplot the observed number of member galaxies and the host stellar mass in Figure 11(a) with colored symbols. Colors indicate the five groups of Δm_{12} . The circle symbols and diamond symbols indicate the LV galaxy groups and the SAGA survey sample, respectively. The LV sample, most of which are from the compilation by Carlsten et al. (2021), consists of 13 galaxy groups of which satellite membership is determined by

measuring their distances using either the TRGB or the SBF method: MW (McConnachie 2012, for compiled data), M31 (Martin et al. 2016; McConnachie 2012; McConnachie et al. 2018, for compiled data), the Local Group (LG; including the MW and M31 subgroups and quasi-isolated outlying members classified by McConnachie (2012)), NGC 2403 (Carlin et al. 2021), NGC 4258 (Kim et al. 2011; Spencer et al. 2014; Carlsten et al. 2021), NGC 4631 (Tanaka et al. 2017; Carlsten et al. 2021), M51 (Carlsten et al. 2021), M101 (Danieli et al. 2017; Bennet et al. 2017, 2019; Carlsten et al. 2019a), M94 (Smercina et al. 2018), NGC 1023 (Trentham & Tully 2009; Carlsten et al. 2021), M104 (Javanmardi et al. 2016; Carlsten et al. 2021), M81 (Chiboucas et al. 2009, 2013), and NGC 5128 (Crnojević et al. 2014, 2019; Müller et al. 2017, 2019). The other galaxy groups that are in Carlsten et al. (2021) compilation but not in this study are excluded either because the spatial coverage is too low (less than 20% of projected virial area is covered) or the SBF signal-to-noise is too low to confirm satellites as faint as $M_r > -12.3$ mag. The SAGA survey sample (Mao et al. 2021) consists of galaxy groups with 36 MW-like host galaxies. The MW-like host galaxies are selected by their K-band

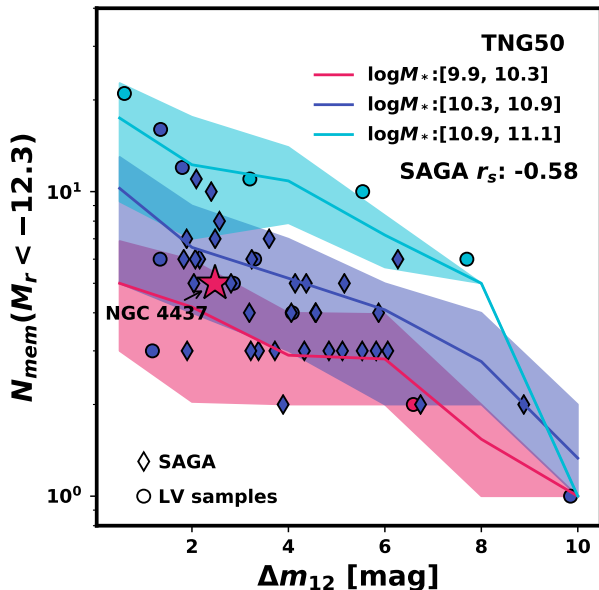


Figure 12. Relations between N_{mem} ($M_r < -12.3$ mag) and Δm_{12} derived from the IllustrisTNG50 simulation, which are divided into three groups by their stellar mass (solid lines with color bands). The star symbol indicates the NGC 4437 group. Diamond symbols and circle symbols show the data from the SAGA survey (Mao et al. 2021) and the LV sample (Carlsten et al. 2021; Carlin et al. 2021; McConnachie 2012; McConnachie et al. 2018).

magnitudes ($-24.6 < M_K < -23$ mag). The SAGA survey covered more than 80% of the projected $R_h = 300$ kpc area and confirmed satellite memberships from their redshifts. It is considered complete to satellites brighter than $M_r = -12.3$ mag. Note that while the spatial coverage of the LV sample significantly differs from galaxy to galaxy and most of them cover less than the virial area, the SAGA survey sample has a relatively consistent spatial coverage.

Most of the references gave luminosities in bandpasses other than r -band. We converted the V -band magnitudes to r -band magnitudes using $M_V = M_r + 0.23$ (Engler et al. 2021). For SAGA hosts, we transformed M_K magnitudes to M_r magnitudes using magnitude relations in TNG100 derived using 44 MW-like subhalos with the same M_K range with SAGA selection criteria, $M_r = M_K + 2.48$ (rms = 0.05 mag). The MW-like subhalos are selected using the g, r, i, z magnitudes of the MW (Bland-Hawthorn, & Gerhard 2016).

Although with a large scatter, the observed galaxy groups generally follow the simulated group lines. Also, the positive correlation between the N_{mem} and the host galaxy stellar mass and the anticorrelation between the

N_{mem} and the Δm_{12} exists for observed galaxy group samples.

Figure 12 illustrates N_{mem} as a function of Δm_{12} for the same simulated and observed samples as in Figure 11. To account for host galaxy stellar mass, we sort our compiled sample into three mass groups according to their host stellar masses as defined in Section 4.2: NGC 4437-like ($9.9 < \log[M_*/M_\odot] < 10.3$, pink), MW-like ($10.3 < \log[M_*/M_\odot] < 10.9$, purple), and massive groups ($10.9 < \log[M_*/M_\odot] < 11.1$, skyblue). A majority of the galaxy groups belong to the MW-like groups.

Among the galaxy groups in the same mass range, the observational data for the groups show clearly a correlation between the number of satellites and Δm_{12} : the smaller the Δm_{12} , the richer the satellite system. The more massive groups have a larger N_{mem} for given Δm_{12} , although the sample numbers in the massive groups and the low-mass groups are small. Again, the observed data generally follow the simulated group lines. The Spearman rank correlation coefficient between Δm_{12} and N_{mem} of the SAGA sample (which is a dominant component of the MW-like groups) is $r_s = -0.58$ (p -value = 3.7×10^{-4}), which confirms that Δm_{12} and N_{mem} are anticorrelated.

We check this correlation in higher resolution simulations, the FIRE project (Hopkins et al. 2014, 2018), a suite of high-resolution zoom-in simulation for MW-like galaxies. In their study of the relation between merger history and satellite populations of eight nearby MW-like galaxies, Smercina et al. (2021) defined the stellar mass of the dominant merger ($M_{*,Dom}$, defined as the greater of either total accreted stellar mass ($M_{*,acc}$) or stellar mass of the most massive satellite ($M_{*,Dom,Sat}$)). They suggested that $M_{*,Dom}$ shows no clear correlation with the number of satellites (N_{sat} for $M_V < -9$ mag) in the FIRE simulation data, while it shows a strong correlation in the observational data (see their Figure 3). Note that the FIRE data used in their study cover a much smaller mass range of $\log M_{*,Dom}/M_\odot$ (9 – 10.3) than the observational data ($\log M_{*,Dom}/M_\odot = 8.5 - 11$).

Using the information of the FIRE sample in Table 3 of Smercina et al. (2021) we investigate relations between merger mass indicators ($M_{*,Dom,Sat}$ and $M_{*,acc}$) and the number of satellites (N_{sat}) in a group. Figure 13(a) shows a positive correlation ($r_s = 0.55$, p -value=0.06) between $M_{*,Dom,Sat}$ and the N_{sat} . However, there is a weak anti-correlation ($r_s = -0.45$, p -value=0.14) between $M_{*,acc}$ and the N_{sat} in Figure 13(b). As a consequence, $M_{*,Dom}$ shows no correlation with N_{sat} ($r_s = -0.17$, p -value=0.59).

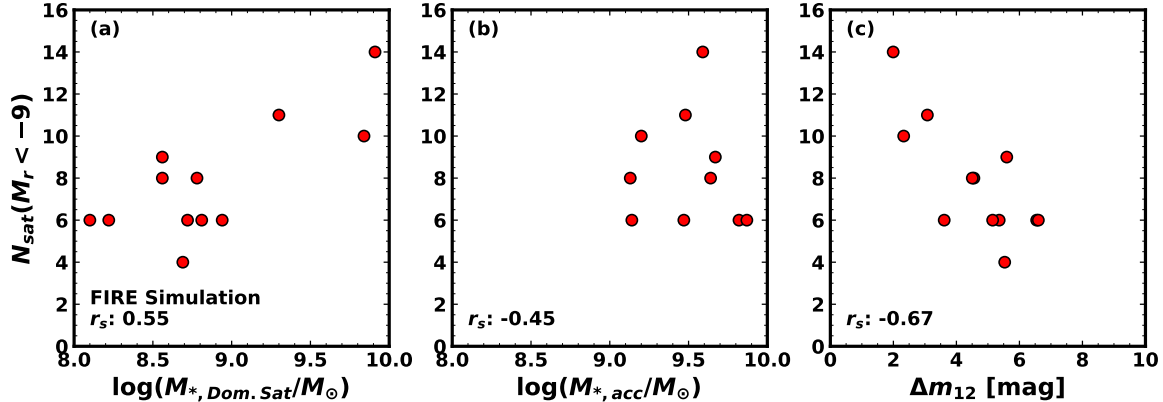


Figure 13. Relations of (a) $M_{*,Dom.Sat}$, (b) $M_{*,acc}$, and (c) Δm_{12} with $N_{sat}(M_r < -9)$, the number of satellites brighter than $M_r = -9$ mag for mock galaxies in the FIRE simulation (data from Table 3 in Smercina et al. (2021)). Spearman correlation coefficients r_s are given in each panel. Here Δm_{12} corresponds to the stellar mass ratio of the host and the most dominant satellite.

If we use the stellar mass ratio between the host galaxy and the most massive satellite galaxy ($M_{*,Dom.Sat}/M_{*,host}$), which is equivalent to Δm_{12} assuming a constant mass-to-light ratio, we find a stronger correlation between $M_{*,Dom.Sat}/M_{*,host}$ and N_{sat} ($r_s = -0.67$, p -value=0.02) as seen in Figure 13(c). Thus it is shown that the number of satellites increases as the the mass ratio between the host galaxy and the most massive satellite galaxy decreases (or as their magnitude gap Δm_{12} increases). This result is consistent with those from observational data and IllustrisTNG50 data in this study (as in Figure 11).

In summary, both observational data and simulation data show that there is a strong correlation among the three parameters of the galaxy groups: the number of member galaxies is correlated with host galaxy stellar mass and with Δm_{12} .

5.3. Magnitude Gap as an Indicator for Galaxy Assembly History

Since the magnitude gap is correlated with the number of member galaxies as well as with host galaxy stellar mass, it is likely to also correlate with group assembly histories. If most of the group mass has assembled at an early epoch and no bright galaxy accreted since then, the galaxy group might lack bright satellites at present. If a bright satellite existed in the group, it would have been already cannibalized by the host galaxy. Therefore, Δm_{12} is likely to be related to mass accretion history.

This view is supported by the previous studies of fossil groups, which are generally defined as massive systems ($M_{r,host} < -21.5$ mag by Raouf et al. (2014)) with a large magnitude gap ($\Delta m_{12} > 2$ mag). The fossil groups are known to have earlier formation times and lack re-

cent satellite accretion (D’Onghia et al. 2005; Kundert et al. 2017). However, the correlation between Δm_{12} and assembly history for galaxy groups with lower mass than the fossil groups is not well-established.

In this subsection, we investigate host galaxy assembly histories as a function of Δm_{12} , across a wide host mass range. In particular, we examine cumulative total mass and stellar mass assembly histories, halo formation times, and stellar-to-halo mass ratios (SHMRs; the ratio of the total stellar mass to the total mass (including dark matter halos)) of host galaxies in relation to Δm_{12} . For this purpose we use the group catalogs from IllustrisTNG50, as described in the previous subsection. From now on, we consider galaxy groups of which the second brightest galaxy is brighter than $M_r = -11$ mag, which is the magnitude limit in our survey of the NGC 4437 group. As before, we divide our galaxy groups into three groups according to their host stellar mass: low-mass groups ($9.9 < \log[M_*/M_\odot] < 10.3$; $N = 306$), MW-like groups ($10.3 < \log[M_*/M_\odot] < 10.9$; $N = 241$), and massive groups ($10.9 < \log[M_*/M_\odot] < 11.5$; $N = 101$), and examine their median properties. In each mass group, we divide simulated galaxy groups into five groups according to Δm_{12} .

The upper and lower panels of Figure 14 display total mass and stellar mass assembly histories (mass fraction with respect to the current mass as a function of redshift) of the galaxy groups. The black lines indicate the median assembly history of all groups. Less massive groups (left and middle panels) assemble, on average, their total mass at an earlier epoch compared to more massive groups (right panel). This tendency is the opposite for the stellar mass assembly history. Less massive groups assemble their stellar mass at a later epoch, since

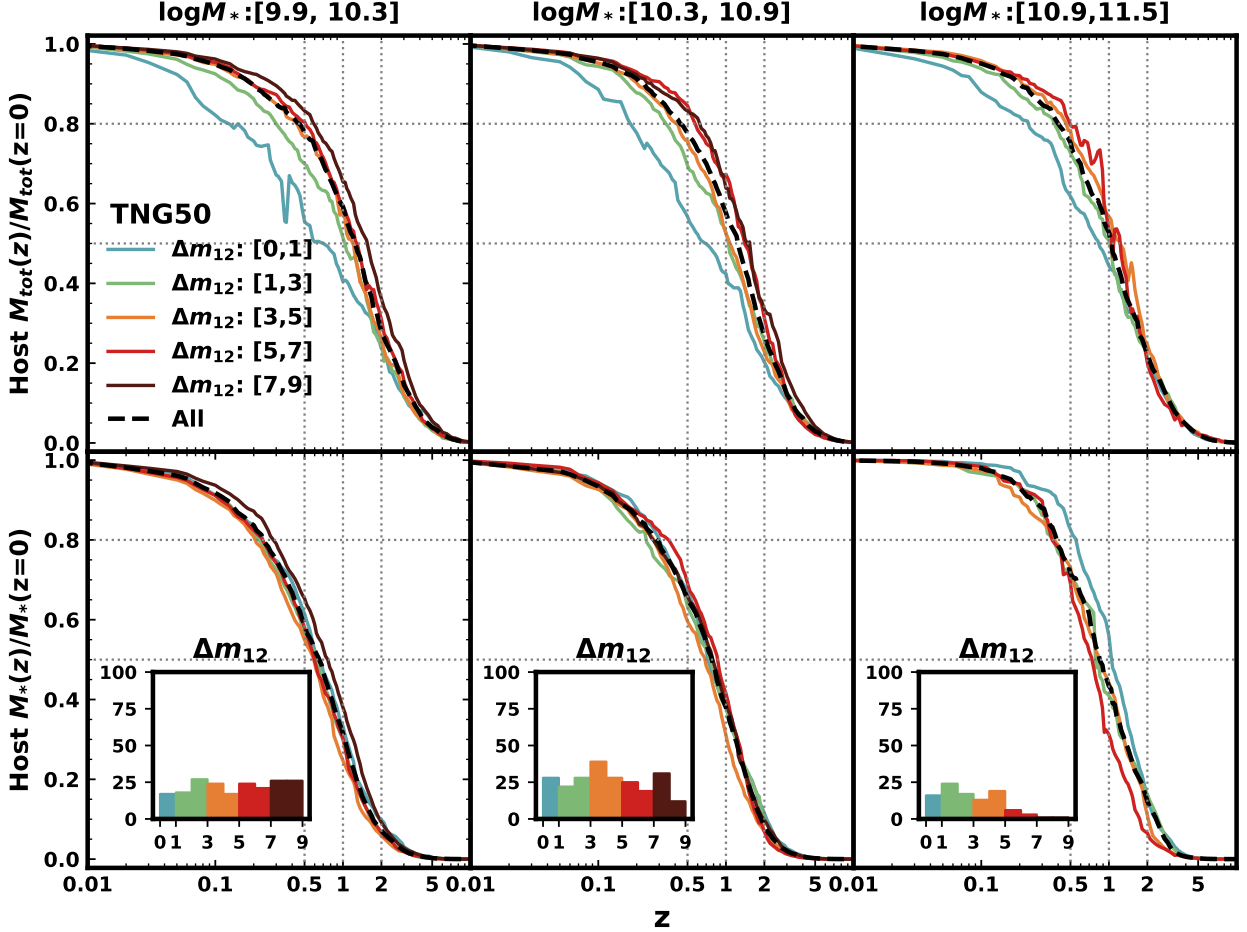


Figure 14. Normalized total mass (upper panels) and stellar mass (lower panels) assembly histories of the host galaxies in different stellar mass ranges ($\log M_*/M_\odot$: [9.9, 10.3] (low-mass groups), [10.3, 10.9] (MW-like groups), and [10.9, 11.5] (massive groups) from left to right, respectively) from the IllustrisTNG50. The median assembly history in each host stellar mass range is indicated as black lines and those divided according to Δm_{12} range are shown as colored lines. Histograms in the lower panels show the distributions of Δm_{12} . In general, galaxy groups with larger Δm_{12} tend to have assembled their total mass earlier, while there is no significant trends in stellar mass assembly.

most host galaxies of low-mass groups show continuous star formation until present day while those of massive groups are quenched.

The distributions of Δm_{12} are shown in the histograms of Figure 14. For the MW-like and massive groups, the number of groups decreases with increasing Δm_{12} . In contrast, many of the low-mass galaxies have a large Δm_{12} .

We plot the median assembly history of each group divided according to Δm_{12} with different colors (the bluer for the smaller Δm_{12}). Host galaxies with large Δm_{12} assemble their total mass earlier than those with small Δm_{12} , in all three mass groups. This suggests that Δm_{12} is a useful parameter that distinguishes different total mass assembly histories. On the other hand, no

such trend exists for stellar mass assembly histories, as shown in the lower panels.

Next, we compare halo formation times of groups with different Δm_{12} . The halo formation time is useful for parameterizing galaxy assembly histories. Here, we examine two parameters, z_{50} and z_{80} . z_{50} (z_{80}) is a redshift at which the host galaxy assembled 50% (80%) of its mass.

The left panels of Figure 15 display relations between Δm_{12} and z_{50} . We show three mass groups separately at the top, middle, and bottom panels. Colors indicate the number of satellite galaxies with $M_r < -11$ mag. There are positive correlations between Δm_{12} and z_{50} in all three mass groups, with $r_s \sim 0.4$. Host galaxies of the galaxy groups with a smaller Δm_{12} have a larger number of satellites and have assembled their total mass

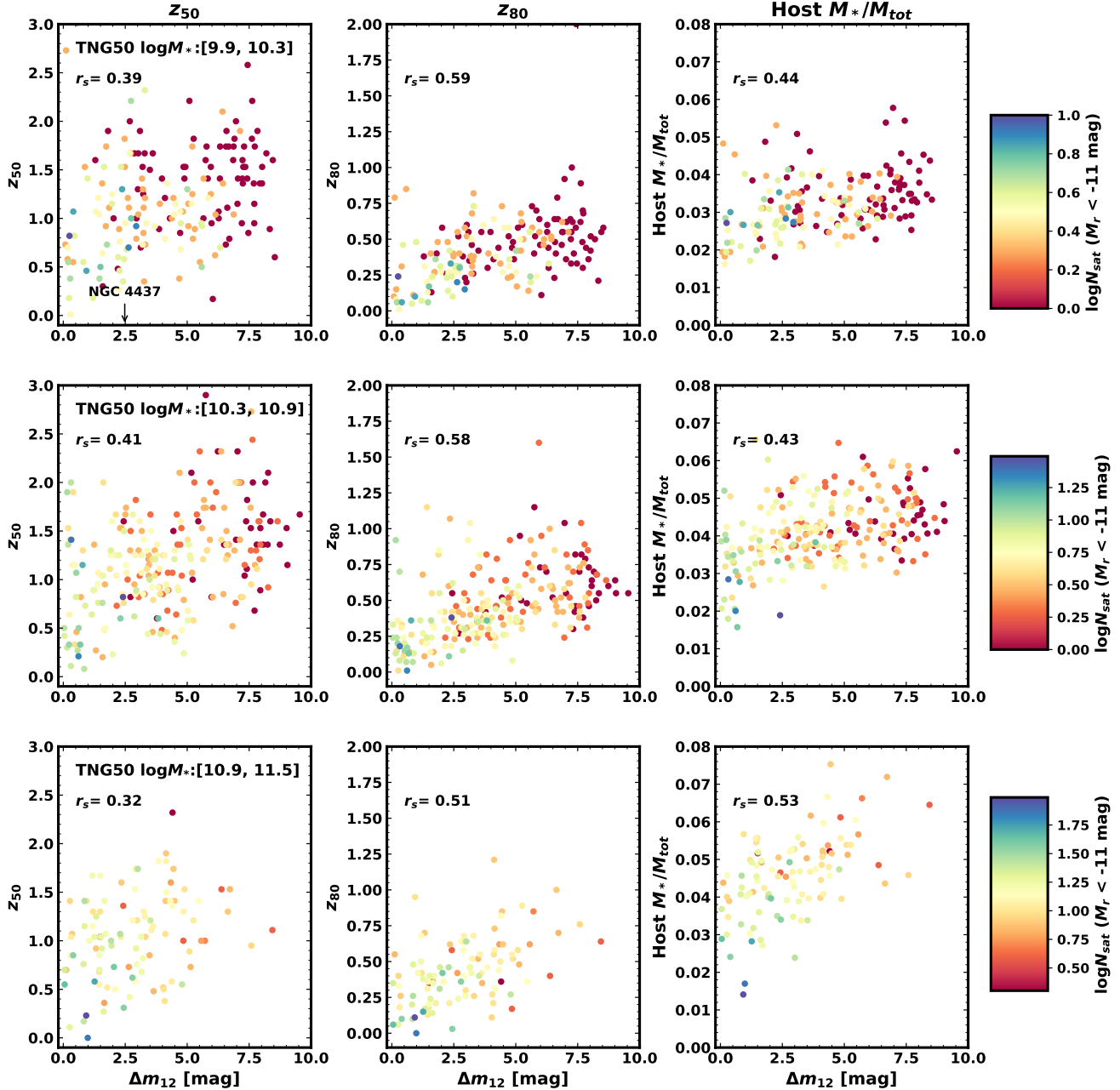


Figure 15. Halo formation times (z_{50} (left panels) and z_{80} (center panels)) and SHMR (right panels) vs. Δm_{12} of the low-mass (top panels), MW-like (middle panels), and massive (bottom panels) groups in the IllustrisTNG50. Colors denote the number of satellite galaxies brighter than $M_r = -11$ mag. The Spearman correlation coefficients (r_s) are displayed in each panel. The magnitude gap of NGC 4437 is annotated as a black arrow on the top left panel.

recently. For instance, 80% of low-mass galaxy groups with $7 < \Delta m_{12} < 9$ have assembled a half of the mass as early as at $z > 1$, while only 40% of low-mass groups with $\Delta m_{12} < 3$ have assembled a half of the mass at $z > 1$. From this, it is inferred that NGC 4437 with small magnitude gap ($\Delta m_{12} = 2.5$ mag) is likely to have

assembled its mass later than other host galaxies with a large magnitude gap.

The middle panels show the relations between Δm_{12} and z_{80} . The correlations for z_{80} are stronger ($r_s \geq 0.5$) compared to z_{50} . This is consistent with the findings from Kundert et al. (2017) that assembly history of fossil groups and nonfossil groups differs more in recent ac-

cretion history and that z_{80} is a more useful parameter than z_{50} in distinguishing them.

The panels in the right represent SHMRs of host galaxies as a function of Δm_{12} . In all three mass groups, positive correlations exist between the two parameters. The correlation is stronger for more massive groups. This is consistent with previous findings that SHMRs of fossil groups are larger than those of nonfossil groups, based on both observations and simulations (Harrison et al. 2012; Kundert et al. 2017). For low-mass groups, SHMRs span relatively a narrow range, meaning that halo masses are not much varied given stellar mass. The correlations are weaker and thus Δm_{12} does not likely to inform much about SHMRs, not to the same degree as does for higher masses.

To summarize, Δm_{12} informs halo formation times and SHMRs of host galaxies even for low-mass groups, in the same manner that can be inferred from the studies of fossil groups: galaxy groups with a large Δm_{12} tend to have a small number of satellites, have assembled at an early epoch, and have a large SHMR. A large diversity in the number of satellites of nearby galaxies partially originate from diverse assembly histories and an easily observable parameter, Δm_{12} , can be used as an indicator for assembly times.

Note that the simulated galaxy groups we use to derive correlations in Figure 15 are spatially more complete than most observed samples. We investigate the relation between the survey coverage and the Spearman correlation coefficients in Figure 16. We derive Spearman correlation coefficients five times using different radius limits for defining a group, $R_h = 150, 200, 250, 300,$ and 500 kpc. Δm_{12} and N_{mem} are determined within each radius limit. In the left panel we show the correlation coefficients between Δm_{12} and N_{mem} ($r_s(\Delta m_{12}, N_{mem})$), and in the right panel Δm_{12} and z_{80} ($r_s(\Delta m_{12}, z_{80})$). We plot the correlation coefficients for three different mass ranges with colored circle symbols and the median virial radii as vertical dotted lines. The absolute values of correlations generally increase as radius limit increases, for both panels. The correlations are not significant if the satellite galaxies are searched only in the virial radius. Thus, for Δm_{12} to be useful for inferring galaxy assembly histories, it is recommended that satellite galaxies are searched in a wide area as large as $\sim 2R_{vir}$.

6. SUMMARY

NGC 4437 is a low-mass edge-on spiral galaxy ($M_r = -20.7$ mag) paired with a dwarf spiral galaxy, NGC 4592 ($M_r = -18.3$ mag). We searched for dwarf galaxies in the $5^\circ \times 4^\circ$ area around NGC 4437 in the WIDE layer of

HSC-SSP (Figure 2) and found 17 satellite candidates (Figure 1 and Table 2). Our automated detection and visual search are approximately complete down to $M_r = -11$ mag and covers $5R_{vir} \times 4R_{vir}$. Then we applied SBF techniques to estimate the distances to the satellite candidates and confirm their membership. Our main results are summarized as follows.

1. *Group membership confirmation.* Based on the SBF distances, we confirm five dwarf galaxies (Dw3, Dw4, Dw12, Dw15, and Dw16) as members of the NGC 4437 group. We try measuring the SBF with five masking thresholds for eliminating contaminating sources, $m_{g,thres} = 26.3, 25.8, 25.3, 24.8,$ and 24.3 mag. From the fluctuation – color diagram, we select five galaxies as likely members and the other twelve as likely background galaxies.
2. *Environmental quenching for low-mass systems.* The two dwarf galaxies, Dw4 and Dw15, that are located at the shorter projected distance to NGC 4437 and NGC 4592, consist of old stellar populations while the other three show star-forming regions. This is consistent with previous findings that environmental quenching plays an important role for low-mass galaxy groups.
3. *Satellite richness of the NGC 4437 group.* Although NGC 4437 is an order of magnitude fainter than the MW, it has a similar number of satellites to those of MW-like galaxy groups. It has a richer satellite system than simulated galaxy groups from IllustrisTNG50, selected by host stellar masses $9.9 < \log M_*/M_\odot < 10.3$. However, it has a typical number of satellites when compared with galaxy groups of similar Δm_{12} , defined as an r -band magnitude difference between the first and the second brightest galaxies.
4. *Magnitude gap and the number of member galaxies.* We find a stratification of the number of member galaxies by Δm_{12} : the smaller the Δm_{12} , the larger the number of satellites. This trend is seen both in IllustrisTNG50 (as well as FIRE) simulations and in observed galaxies sample (Figure 11).
5. *Magnitude gap and the galaxy assembly history.* From simulated spatially-complete galaxy groups in IllustrisTNG50, we find that galaxy groups (for host galaxy stellar mass range $9.9 < \log M_*/M_\odot < 11.5$) with smaller Δm_{12} assemble their total mass at a later epoch (Figure 14). Thus, they have relatively later halo formation times z_{50} and z_{80} , with

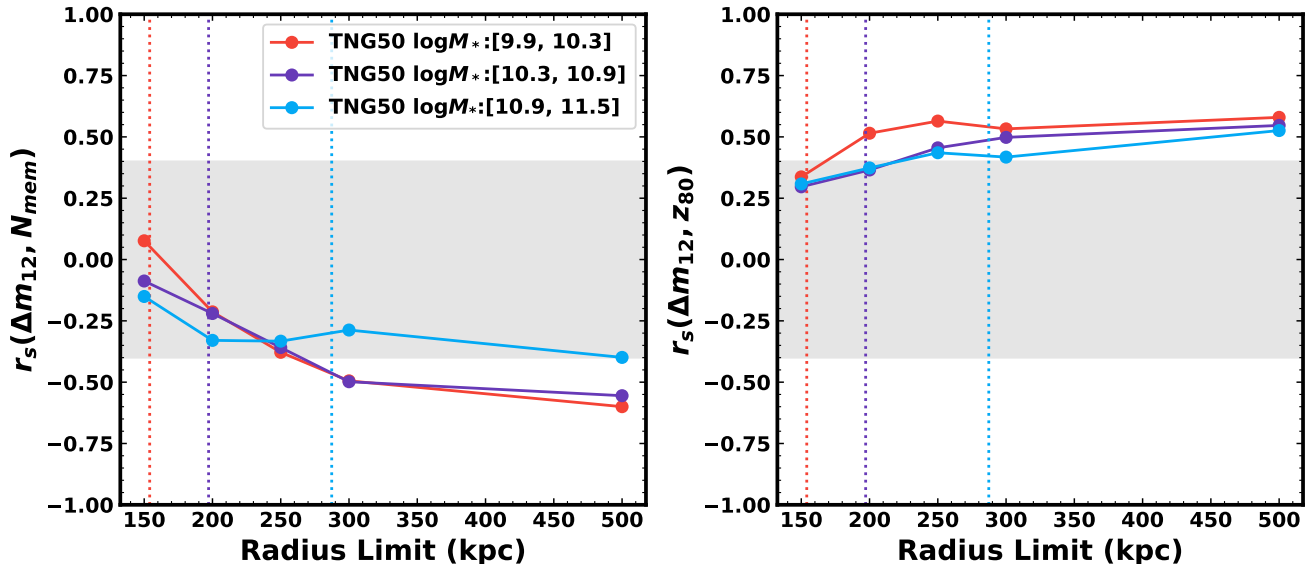


Figure 16. Spearman correlation coefficients between Δm_{12} and N_{mem} (left) and Δm_{12} and z_{80} (right), as a function of radius limits for defining a group. Vertical lines indicate the average virial radius of each groups of mass range. For all the three mass ranges, the correlations increase as radius limit increases.

z_{80} being more tightly correlated to Δm_{12} . While SHMR is correlated significantly with Δm_{12} for massive groups ($10.9 < \log M_*/M_\odot < 11.5$), the correlation gets weaker with decreasing host stellar mass (Figure 15). These findings imply that Δm_{12} provides information about assembly histories even for low-mass groups and the diverse assembly histories may account for a large scatter in observed satellite number of nearby galaxy groups. In addition, the correlations increase as the radius limit for group definition increases, showing that

satellite galaxies should be searched in a wide area to use Δm_{12} as an indicator for galaxy assembly.

ACKNOWLEDGMENTS

This work was supported by the National Research Foundation grant funded by the Korean Government (NRF-2019R1A2C2084019). J.K. was supported by the Global Ph.D. Fellowship Program (NRF-2016H1A2A1907015) of the National Research Foundation. We thank the anonymous referee for providing helpful comments. We thank Brian S. Cho for his help in improving the English in this manuscript.

REFERENCES

- Aguerri, J. A. L. & Zarattini, S. 2021, *Universe*, 7, 132. doi:10.3390/universe7050132
- Aihara, H., Arimoto, N., Armstrong, R., et al. 2018, *PASJ*, 70, S4
- Aihara, H., AlSayyad, Y., Ando, M., et al. 2019, *PASJ*, 71, 114
- Behroozi, P. S., Wechsler, R. H., & Conroy, C. 2013, *ApJ*, 770, 57. doi:10.1088/0004-637X/770/1/57
- Bennet, P., Sand, D. J., Crnojević, D., et al. 2017, *ApJ*, 850, 109. doi:10.3847/1538-4357/aa9180
- Bennet, P., Sand, D. J., Crnojević, D., et al. 2019, *ApJ*, 885, 153. doi:10.3847/1538-4357/ab46ab
- Bertin, E. & Arnouts, S. 1996, *A&AS*, 117, 393. doi:10.1051/aas:1996164
- Blakeslee, J. P., Jensen, J. B., Ma, C.-P., et al. 2021, *ApJ*, 911, 65. doi:10.3847/1538-4357/abe86a
- Bland-Hawthorn, J., & Gerhard, O. 2016, *ARA&A*, 54, 529
- Bosch, J., Armstrong, R., Bickerton, S., et al. 2018, *PASJ*, 70, S5. doi:10.1093/pasj/psx080
- Bullock, J. S. & Boylan-Kolchin, M. 2017, *ARA&A*, 55, 343. doi:10.1146/annurev-astro-091916-055313

- Cantiello, M., Blakeslee, J. P., Ferrarese, L., et al. 2018, *ApJ*, 856, 126
- Carlin, J. L., Sand, D. J., Price, P., et al. 2016, *ApJL*, 828, L5. doi:10.3847/2041-8205/828/1/L5
- Carlin, J. L., Mutlu-Pakdil, B., Crnojević, D., et al. 2021, *ApJ*, 909, 211. doi:10.3847/1538-4357/abe040
- Carlsten, S. G., Beaton, R. L., Greco, J. P., et al. 2019, *ApJ*, 879, 13
- Carlsten, S. G., Beaton, R. L., Greco, J. P., et al. 2019, *ApJL*, 878, L16. doi:10.3847/2041-8213/ab24d2
- Carlsten, S. G., Greco, J. P., Beaton, R. L., et al. 2020, *ApJ*, 891, 144. doi:10.3847/1538-4357/ab7758
- Carlsten, S. G., Greene, J. E., Peter, A. H. G., et al. 2020, *ApJ*, 902, 124. doi:10.3847/1538-4357/abb60b
- Carlsten, S. G., Greene, J. E., Peter, A. H. G., et al. 2021, *ApJ*, 908, 109. doi:10.3847/1538-4357/abd039
- Chiboucas, K., Karachentsev, I. D., & Tully, R. B. 2009, *AJ*, 137, 3009. doi:10.1088/0004-6256/137/2/3009
- Chiboucas, K., Jacobs, B. A., Tully, R. B., et al. 2013, *AJ*, 146, 126. doi:10.1088/0004-6256/146/5/126
- Crnojević, D., Sand, D. J., Caldwell, N., et al. 2014, *ApJL*, 795, L35. doi:10.1088/2041-8205/795/2/L35
- Crnojević, D., Sand, D. J., Bennet, P., et al. 2019, *ApJ*, 872, 80. doi:10.3847/1538-4357/aafbe7
- D’Onghia, E., Sommer-Larsen, J., Romeo, A. D., et al. 2005, *ApJL*, 630, L109. doi:10.1086/491651
- Danieli, S., van Dokkum, P., Merritt, A., et al. 2017, *ApJ*, 837, 136. doi:10.3847/1538-4357/aa615b
- Davis, A. B., Nierenberg, A. M., Peter, A. H. G., et al. 2021, *MNRAS*, 500, 3854. doi:10.1093/mnras/staa3246
- de Vaucouleurs, G., de Vaucouleurs, A., Corwin, H. G., et al. 1991, *Third Reference Catalogue of Bright Galaxies (RC3)* (New York: Springer)
- Dolag, K., Borgani, S., Murante, G., et al. 2009, *MNRAS*, 399, 497. doi:10.1111/j.1365-2966.2009.15034.x
- Dressler, A. 1980, *ApJ*, 236, 351. doi:10.1086/157753
- Einasto, J., Saar, E., Kaasik, A., et al. 1974, *Nature*, 252, 111. doi:10.1038/252111a0
- Engler, C., Pillepich, A., Pasquali, A., et al. 2021, *MNRAS*, 507, 4211. doi:10.1093/mnras/stab2437
- Fattahi, A., Navarro, J. F., Sawala, T., et al. 2016, *MNRAS*, 457, 844. doi:10.1093/mnras/stv2970
- Font, A. S., McCarthy, I. G., & Belokurov, V. 2021, *MNRAS*, 505, 783. doi:10.1093/mnras/stab1332
- Garrison-Kimmel, S., Hopkins, P. F., Wetzel, A., et al. 2019, *MNRAS*, 487, 1380. doi:10.1093/mnras/stz1317
- Geha, M., Wechsler, R. H., Mao, Y.-Y., et al. 2017, *ApJ*, 847, 4. doi:10.3847/1538-4357/aa8626
- Habas, R., Marleau, F. R., Duc, P.-A., et al. 2020, *MNRAS*, 491, 1901. doi:10.1093/mnras/stz3045
- Harrison, C. D., Miller, C. J., Richards, J. W., et al. 2012, *ApJ*, 752, 12. doi:10.1088/0004-637X/752/1/12
- Hearin, A. P., Zentner, A. R., Newman, J. A., et al. 2013, *MNRAS*, 430, 1238. doi:10.1093/mnras/sts699
- Hopkins, P. F., Kereš, D., Oñorbe, J., et al. 2014, *MNRAS*, 445, 581. doi:10.1093/mnras/stu1738
- Hopkins, P. F., Wetzel, A., Kereš, D., et al. 2018, *MNRAS*, 480, 800. doi:10.1093/mnras/sty1690
- Ivezić, Ž., Kahn, S. M., Tyson, J. A., et al. 2019, *ApJ*, 873, 111
- Jarrett, T. H., Chester, T., Cutri, R., et al. 2003, *AJ*, 125, 525. doi:10.1086/345794
- Javanmardi, B., Martinez-Delgado, D., Kroupa, P., et al. 2016, *A&A*, 588, A89. doi:10.1051/0004-6361/201527745
- Jerjen, H., Freeman, K. C., & Binggeli, B. 2000, *AJ*, 119, 166. doi:10.1086/301188
- Jones, L. R., Ponman, T. J., Horton, A., et al. 2003, *MNRAS*, 343, 627. doi:10.1046/j.1365-8711.2003.06702.x
- Karachentsev, I. D., & Nasonova, O. G. 2013, *MNRAS*, 429, 2677
- Karachentsev, I. D., Makarov, D. I., & Kaisina, E. I. 2013, *AJ*, 145, 101. doi:10.1088/0004-6256/145/4/101
- Karachentseva, V. E. 1968, *Soobshcheniya Byurakanskoj Observatorii Akademii Nauk Armyanskoi SSR Erevan*, 39, 62
- Kim, E., Kim, M., Hwang, N., et al. 2011, *MNRAS*, 412, 1881. doi:10.1111/j.1365-2966.2010.18022.x
- Kim, Y. J., Kang, J., Lee, M. G., et al. 2020, *ApJ*, 905, 104. doi:10.3847/1538-4357/abbd9
- Kim, Y. J. & Lee, M. G. 2021, *ApJ*, 923, 152. doi:10.3847/1538-4357/ac2d94
- Klypin, A., Kravtsov, A. V., Valenzuela, O., et al. 1999, *ApJ*, 522, 82. doi:10.1086/307643
- Kondapally, R., Russell, G. A., Conselice, C. J., et al. 2018, *MNRAS*, 481, 1759. doi:10.1093/mnras/sty2333
- Kundert, A., D’Onghia, E., & Aguerrri, J. A. L. 2017, *ApJ*, 845, 45. doi:10.3847/1538-4357/aa7b88
- Liske, J., Lemon, D. J., Driver, S. P., et al. 2003, *MNRAS*, 344, 307
- Maddox, S. J., Sutherland, W. J., Efstathiou, G., et al. 1990, *MNRAS*, 243, 692
- Mao, Y.-Y., Geha, M., Wechsler, R. H., et al. 2021, *ApJ*, 907, 85. doi:10.3847/1538-4357/abce58
- Marinacci, F., Vogelsberger, M., Pakmor, R., et al. 2018, *MNRAS*, 480, 5113. doi:10.1093/mnras/sty2206
- Martin, N. F., Ibata, R. A., Lewis, G. F., et al. 2016, *ApJ*, 833, 167. doi:10.3847/1538-4357/833/2/167
- McConnachie, A. W. 2012, *AJ*, 144, 4. doi:10.1088/0004-6256/144/1/4

- McConnachie, A. W., Ibata, R., Martin, N., et al. 2018, *ApJ*, 868, 55. doi:10.3847/1538-4357/aae8e7
- Mei, S., Blakeslee, J. P., Tonry, J. L., et al. 2005, *ApJS*, 156, 113
- Mei, S., Blakeslee, J. P., Côté, P., et al. 2007, *ApJ*, 655, 144. doi:10.1086/509598
- Metcalfe, N., Fong, R., Shanks, T., et al. 1989, *MNRAS*, 236, 207
- Mieske, S., Hilker, M., Infante, L., et al. 2007, *A&A*, 463, 503. doi:10.1051/0004-6361/20066300
- Moore, B., Ghigna, S., Governato, F., et al. 1999, *ApJL*, 524, L19. doi:10.1086/312287
- Müller, O. & Jerjen, H. 2020, *A&A*, 644, A91. doi:10.1051/0004-6361/202038862
- Müller, O., Rejkuba, M., Pawlowski, M. S., et al. 2019, *A&A*, 629, A18. doi:10.1051/0004-6361/201935807
- Müller, O., Jerjen, H., & Binggeli, B. 2017, *A&A*, 597, A7. doi:10.1051/0004-6361/201628921
- Naiman, J. P., Pillepich, A., Springel, V., et al. 2018, *MNRAS*, 477, 1206. doi:10.1093/mnras/sty618
- Nelson, D., Pillepich, A., Springel, V., et al. 2018, *MNRAS*, 475, 624. doi:10.1093/mnras/stx3040
- Nelson, D., Springel, V., Pillepich, A., et al. 2019, *Computational Astrophysics and Cosmology*, 6, 2. doi:10.1186/s40668-019-0028-x
- Peng, C. Y., Ho, L. C., Impey, C. D., et al. 2002, *AJ*, 124, 266. doi:10.1086/340952
- Pillepich, A., Nelson, D., Hernquist, L., et al. 2018, *MNRAS*, 475, 648. doi:10.1093/mnras/stx3112
- Raouf, M., Khosroshahi, H. G., Ponman, T. J., et al. 2014, *MNRAS*, 442, 1578. doi:10.1093/mnras/stu963
- Roberts, D. M., Nierenberg, A. M., & Peter, A. H. G. 2021, *MNRAS*, 502, 1205. doi:10.1093/mnras/stab069
- Sawala, T., Frenk, C. S., Fattahi, A., et al. 2016, *MNRAS*, 456, 85. doi:10.1093/mnras/stv2597
- Schlafly, E. F., & Finkbeiner, D. P. 2011, *ApJ*, 737, 103
- Schlegel, D. J., Finkbeiner, D. P., & Davis, M. 1998, *ApJ*, 500, 525
- Smercina, A., Bell, E. F., Price, P. A., et al. 2018, *ApJ*, 863, 152. doi:10.3847/1538-4357/aad2d6
- Smercina, A., Bell, E. F., Samuel, J., et al. 2021, arXiv:2107.04591
- Spencer, M., Loebman, S., & Yoachim, P. 2014, *ApJ*, 788, 146. doi:10.1088/0004-637X/788/2/146
- Springel, V., White, S. D. M., Tormen, G., et al. 2001, *MNRAS*, 328, 726. doi:10.1046/j.1365-8711.2001.04912.x
- Springel, V., Pakmor, R., Pillepich, A., et al. 2018, *MNRAS*, 475, 676. doi:10.1093/mnras/stx3304
- Tanaka, M., Chiba, M., & Komiyama, Y. 2017, *ApJ*, 842, 127. doi:10.3847/1538-4357/aa6d11
- Tanaka, M., Chiba, M., Hayashi, K., et al. 2018, *ApJ*, 865, 125. doi:10.3847/1538-4357/aad9fe
- Tonry, J., & Schneider, D. P. 1988, *AJ*, 96, 807
- Trentham, N. & Tully, R. B. 2009, *MNRAS*, 398, 722. doi:10.1111/j.1365-2966.2009.15189.x
- van den Bergh, S. 1994, *ApJ*, 428, 617. doi:10.1086/174270
- Wang, W., Takada, M., Li, X., et al. 2021, *MNRAS*, 500, 3776. doi:10.1093/mnras/staa3495
- Wetzel, A. R., Hopkins, P. F., Kim, J.-hoon., et al. 2016, *ApJL*, 827, L23. doi:10.3847/2041-8205/827/2/L23
- Zwicky, F., Herzog, E., Wild, P., et al. 1961, Pasadena: California Institute of Technology (CIT), —c1961